JOURNAL OF GEOPHYSICAL RESEARCH, VOL. 114, D19106, doi:10.1029/2009JD011775, 2009

Calculating distributed glacier mass balance for the Swiss Alps from regional climate model output: A methodical description and interpretation of the results

H. Machguth,[1] F. Paul,[1] S. Kotlarski,[2,3] and M. Hoelzle[4]

Received 20 January 2009; revised 1 May 2009; accepted 20 July 2009; published 8 October 2009.

[1] This study aims at giving a methodical description of the use of gridded output from a regional climate model (RCM) for the calculation of glacier mass balance distribution for the perimeter of the Swiss Alps. The mass balance model runs at daily steps and 100 m spatial resolution, while the regional model (REMO) RCM provides daily grids (~18 km resolution) of dynamically downscaled reanalysis data. A combination of interpolation techniques and simple subgrid parameterizations is applied to bridge the gap in spatial resolution and to obtain daily input fields of air temperature, global radiation, and precipitation. Interpolation schemes are a key element and thus we test different interpolators. For validation, computed mass balances are compared to stake measurements and time series (1979–2003) of observed mass balance. The meteorological input fields are compared to measurements at weather stations. The applied inverse distance weighting introduces systematic biases due to spatial autocorrelation, whereas thin plate splines preserve the characteristics of the RCM output. While summer melt at point locations on several glaciers is well reproduced by the model, accumulation is mostly underestimated. These systematic shifts are correlated to biases of the meteorological input fields. Time series of mass balance obtained from the model run agree well with observed time series. We conclude that the gap in spatial resolution is not a major drawback, given that interpolators and parameterizations are selected upon detailed considerations. Biases in RCM precipitation are a major source for the observed underestimations in mass balance and have to be corrected prior to operational use of the presented approach.

Citation: Machguth, H., F. Paul, S. Kotlarski, and M. Hoelzle (2009), Calculating distributed glacier mass balance for the Swiss Alps from regional climate model output: A methodical description and interpretation of the results, *J. Geophys. Res.*, *114*, D19106, doi:10.1029/2009JD011775.

1. Introduction

[2] The possible disappearance of glaciers under future climatic conditions is a major concern and numerous studies have assessed expected glacier changes from a wide range of approaches. As glacier mass balance is closely linked to annual meteorological conditions, mass balance is a key feature in understanding the glacier-climate relationship. Consequently, mass balance modeling has been subject to a wealth of studies, ranging from very detailed process orientated approaches with sophisticated models operating at the point scale, to distributed and less complex models applied to entire glaciers and/or samples of several glaciers (see *Oerlemans* [2001] and *Greuell and Genthon* [2004] for an overview). Thereby, the level of model complexity largely depends on the research question and the available data to run the model.

[3] With respect to climate change impact assessment, there is need to cover entire glacierized mountain ranges at a sufficient level of detail. Two major challenges have to be faced when modeling glacier mass balances in rugged high-mountain terrain: the small number of measurements (e.g., climate stations) in most glacierized regions in the world and the spatial extrapolation of the meteorological input parameters from these measurements at point locations. In principal, regional climate models (RCMs) are able to provide the three basic drivers of glacier mass balance, temperature (T_a), precipitation (P), and global radiation (S_{in}) over large regions by dynamical downscaling of general circulation model (GCM) or reanalysis data to about 10–50 km spatial resolution. Their most important advantage is the possibility to generate physically consistent fields of atmospheric variables for an entire region and for today's climatic conditions as well as for climate scenarios [*Salzmann et al.*, 2007]. However, their main drawback

[1]Physical Geography Division, Department of Geography, University of Zurich, Zurich, Switzerland.
[2]Max Planck Institute for Meteorology, Hamburg, Germany.
[3]Now at Institute for Atmospheric and Climate Science, ETH Zurich, Zurich, Switzerland.
[4]Department of Geoscience, University of Fribourg, Fribourg, Switzerland.

0148-0227/09/2009JD011775$09.00

is the coarse spatial resolution. Distributed mass balance calculation in rugged high-mountain topography is usually performed at 25–100 m spatial resolution to account for small-scale variability (e.g., slope and aspect, shading). Furthermore, local meteorological phenomena at a scale of less than one to a few kilometers (e.g., orographic precipitation) are also relevant to mass balance distribution and are not resolved by the RCMs.

[4] Indeed, the scale mismatch is a problem in many studies related to climate change impact assessment on regional to local scales. Previous studies that have utilized output from climate models for mass balance calculations were mostly focused on individual glaciers, acquiring data from the nearest climate model grid box in combination with a statistical downscaling [e.g., *Van de Wal and Wild*, 2001; *Schneeberger et al.*, 2003; *Radić and Hock*, 2006; *Stahl et al.*, 2008]. Other studies used the meteorological fields from several grid boxes at the same time and performed mass balance computations directly at the spatial resolution of the RCM [e.g., *Bhatt et al.*, 2007; *Cook et al.*, 2003; *Ren et al.*, 2007; *Zhang et al.*, 2007]. However, so far no attempt was made to downscale a whole field of RCM output to a higher resolution and to apply these data for mass balance computation.

[5] In this study we give a methodical description of a coupling scheme between RCM data and a mass balance model which is designed to compute mass balance distribution over entire mountain ranges, i.e., at the regional scale. Output from the RCM REMO [e.g., *Jacob et al.*, 2001] is downscaled from about 18 km to 100 m and then used as an input for a 24-year transient run of a distributed glacier mass balance model for the entire Swiss Alps. More specifically, we describe different methods of spatial inter/extrapolation of the RCM data and illustrate different ways of validating the model input (i.e., the downscaled field of RCM data) as well as the model output (i.e., the mass balance distribution). The underlying principle is to apply the RCM data without bias corrections in order to identify their limits and allow for a comprehensive description of the methodical steps.

[6] The paper is organized in the following way: Basic considerations on how to apply RCM data for mass balance calculation are raised in section 2. Afterward the model domain and the applied data are presented in section 3. The technical description of mass balance calculation in section 4 includes the mass balance model and the explanation of the downscaling scheme for the RCM data. The results are then presented in section 5, followed by section 6, which focuses on a technical analysis of the results with respect to the chosen parameterizations of mass balance computation and the RCM downscaling scheme. In section 7, the results are discussed in the broader context of overall model performance and its applicability for operational use. Finally, conclusions are drawn and an outlook is given in section 8.

2. Basic Considerations of Applying RCM Data

[7] In this study the mass balance of a large sample of individual glaciers is modeled explicitly, i.e., with their topography as represented in a 100 m resolution digital terrain model (DTM), and the numerical time steps of the computation are chosen to be 1 day. The size of the model domain (the Swiss Alps, 300 × 200 km) implies that meteorological fields have to be used instead of data from individual weather stations [e.g., *Klok and Oerlemans*, 2002] or selected grid boxes from climate model output [e.g., *Schneeberger et al.*, 2003]. The spatial and temporal resolution of the required meteorological fields should be similar to the mass balance model.

[8] Apart from reanalysis data, there are two possible sources of meteorological fields: gridded climatologies derived from measurements or RCM output. Neither of them has a resolution similar to the mass balance model both temporally and spatially. It was decided to work with RCM data for the following reasons: RCM data are available at high temporal resolution (subdaily) and provide physically consistent fields whereas the available gridded climatologies [e.g., *Böhm et al.*, 2001; *Schwarb et al.*, 2001, Plate 2.6; *Meerkötter et al.*, 2004; *Auer et al.*, 2007] are of differing spatial and temporal resolution and extent. Furthermore, given that a coupling scheme between RCM data and the mass balance model can be found, this would allow to use data from RCM climate-scenario runs. However, RCM data are biased [e.g., *Kotlarski et al.*, 2009]. Although often used as a reference to RCM data, gridded climatologies are also not free of errors, in particular in high-mountain regions where measurements are sparse. Indeed, it would be interesting to combine both data sources, for instance to correct biases in the RCM data. Nevertheless, here we focus on RCM output and apply a gridded climatology only to validate the RCM data. We believe that a more comprehensive incorporation of gridded climatologies should be the objective of pursuing studies. The use of uncorrected RCM data also allows better assessment of the potential of regional-scale glacier mass balance modeling when applied to regions with limited observational data.

[9] In this study, the mass balance model is driven by the RCM output through an offline coupling scheme and there is no feedback to the RCM. The spatial resolution of the RCM output is increased to the resolution of the mass balance model (100 m) through a combination of interpolation techniques and parameterizations which account for the variability on a subgrid scale. The RCM output is treated as a gridded field of virtual climate stations at the grid box elevations. In a first step, this coarse field which accounts for large-scale variability of the meteorological conditions is smoothed by means of interpolation techniques. We applied different interpolators to determine their influence on modeled mass balance. In a second step, the variability on a subgrid scale is accounted for by means of simple subgrid parameterizations. The applied parameterizations are different for each of the three variables (T_a, P and S_{in}) as their spatial variability is different and because they do not depend on the same factors. The RCM values are rescaled to a higher-resolution DTM by combining the altitudinal gradients for T_a and P (Γ_{Ta} and Γ_P) with the RCM grid box elevations. While the dependency of T_a with altitude is rather strict, it is less pronounced for P: Precipitation gradients are spatially variable [*Sevruk*, 1997] and measurements of solid precipitation at the elevation of glaciers (here >2000 m asl (meters above sea level)) are highly uncertain [e.g., *Sevruk*, 1985, 1997]. For S_{in}, the modeling approach is twofold: the RCM provides the cloud cover over a larger region while a radiation code [e.g., *Corripio*, 2003] based

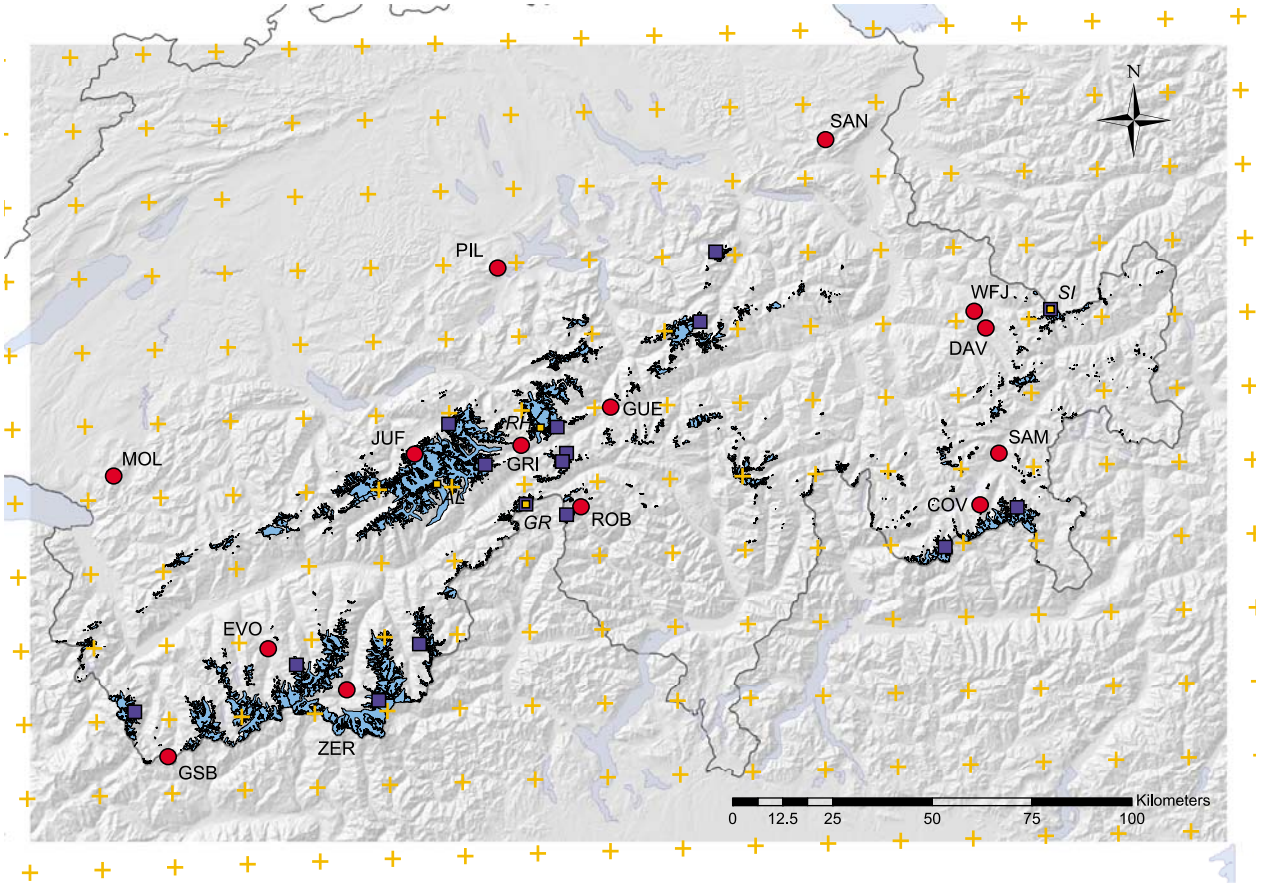

Figure 1. Model domain, from ~6°40′E–10°35′E and ~45°40′N–47°30′N, with the full DTM. Glaciers are in light blue, and glaciers with available stake measurements are marked with blue squares. Small orange squares mark glaciers where results of this study have been compared to data from *Huss et al.* [2008]. Abbreviations (in italic) refer to: AL, Great Aletsch glacier; RH, Rhône glacier; GR, Gries glacier; and SI, Silvretta glacier. Orange pluses denote the centers of the REMO grid boxes. Red dots show locations of the MeteoSwiss weather stations used for validation (altitude in m asl): COV, Corvatsch, 3315; DAV, Davos, 1590; EVO, Evolène, 1825; GRI, Grimsel-Hospiz, 1980; GSB, Grand-Saint-Bernard, 2472; GUE, Gütsch, 2287; JUF, Jungfraujoch, 3580; MOL, Molèson, 1972; PIL, Pilatus, 2106; ROB, Robiei, 1898; SAM, Samedan, 1705; SAN, Säntis, 2490; WFJ, Weissfluhjoch, 2690; and ZER, Zermatt, 1638. For orientation, the border of Switzerland is shown in black and lakes are light blue.

on the 100 m resolution DTM gives the spatial variability of the potential (i.e., clear-sky) global radiation for each day of the year. This approach allows to consider topographic influences on global radiation accurately while maintaining the overall reduction due to clouds [*Paul et al.*, 2008].

[10] The applied downscaling procedure includes simplified parameterizations. To test their performance and to allow for a better assessment of the modeled mass balance distribution, the downscaled fields of S_{in}, T_a and P (i.e., the model input) are compared to measurements. These downscaled fields are in the following indicated with a hat: $\hat{T}_a$, $\hat{P}$, $\hat{S}_{in}$. The same notation is also applied to cloudiness (n) and the native REMO topography ($\mathrm{DTM_{REMO}}$) ($\hat{n}$ and $\widehat{\mathrm{DTM}}_{\mathrm{REMO}}$ after interpolation to 100 m).

3. Model Domain and Data

3.1. Spatial and Temporal Model Domain

[11] The mass balance calculation is applied to the entire Swiss Alps which cover an area of approximately 25000 km^2. Together with adjacent areas they are represented by a DTM of 3000 × 2000 cells at a spatial resolution of 100 m (Figure 1). The DTM is a composite of two DTMs, both resampled to 100 m horizontal resolution: the Swiss Alps (including all the modeled glaciers) are represented by the DTM25 level2 from swisstopo (a DTM with 25 m resolution and glacier surfaces mostly from the mid-1990s) and the surrounding terrain by the SRTM 90 m DTM which was acquired in the year 2000.

[12] The present study uses digital outlines from the Swiss Glacier Inventory from 1973 [*Müller et al.*, 1976] which is the most complete data set with respect to glacier polygons currently available for the area of interest. The glacierized area in Switzerland was 1280 km^2 at that time and consisted of approximately 2000 individual glaciers [*Müller et al.*, 1976; *Paul et al.*, 2004]. Glaciers of sufficient size (>1 km^2) are located within a perimeter reaching from 45.9°N–47.0°N and from 6.9°E–10.4°E (Figure 1). The digital glacier polygons applied in this study are based upon the inventory from *Müller et al.* [1976] which was revised

by *Maisch et al.* [2000] and *Wipf* [1999] and digitized in the framework of the new Swiss glacier inventory project [*Paul*, 2007]. The digital glacier polygons have a unique index and for the mass balance computation, a rasterized glacier mask (100 m grid spacing) is created by assigning the indices to all the grid cells being located within the corresponding glacier polygon. Both the DTM and the glacier polygons are given in the conformal Swiss geodetic projection.

[13] The temporal model domain was chosen to be 25 September 1979 until 5 October 2003. In the following, this time span is referred to as the calculation period. Thus, the model runs are conducted over 24 mass balance years. A mass balance year is defined here as starting 1 October and ending 30 September and is further divided into winter balance (1 October to 30 April) and summer balance (1 May to 30 September).

3.2. Input Data

[14] The mass balance model is driven by the output of the hydrostatic RCM REMO (version 5.5) developed by the Max Planck Institute for Meteorology, Hamburg [e.g., *Jacob et al.*, 2001]. REMO was selected because studies on the uncertainties in REMO exist [e.g., *Kotlarski et al.*, 2005], its performance in high-elevation regions of the European Alps has been evaluated by *Kotlarski et al.* [2009] and first mass balance calculations using REMO output have been performed as well (F. Paul and S. Kotlarski, Forcing a distributed mass balance model with the regional climate model REMO, part II: Downscaling strategy and first results, submitted to *Journal of Climate*, 2009). In this study we use the output from a model run conducted over a larger portion of central Europe (reaching from approximately 41°N–50°N and from 1°W–17°E) at a spatial resolution of 1/6° (~18 km) on a rotated spherical grid. The experiment covers the time span 1958–2003. At the lateral boundaries REMO is driven by ERA40 reanalysis data [*Uppala et al.*, 2005] (from 1 January 1958 to 31 July 2002) and by the operational analysis of the ECMWF (1 August 2002 to 31 December 2003). The internal model time step is 100 s and the model output is stored as hourly means. From the latter daily means and sums are computed and used in this study. For the mass balance computation, we use REMO output on 2 m air temperature (T_a), precipitation (P) and cloudiness (n).

3.3. Data for Validation

[15] The downscaled parameters $\hat{T}_a$, $\hat{P}$ (see section 4.2), $\hat{S}_{in}$ (see section 4.1.3) are compared to measurements. For the time period 1 January 1981 to 31 December 2003 we acquired daily means of measured S_{in}, P and T_a from 14 weather stations in the Swiss Alps (Figure 1). The stations are all operated by MeteoSwiss and are located at elevations from 1590 to 3580 m asl. The sample size consists of summit stations, stations on passes and valley stations. Furthermore $\hat{P}$ over the glacierized area is compared to the *Schwarb et al.* [2001, Plate 2.6] precipitation climatology.

[16] Modeled values of mass balance are compared to stake measurements on 16 different glaciers (Figure 1). The data sets have been acquired from *Müller and Kappenberger* [1991] (1 glacier) and *Cryospheric Commission* [1992–2008] (3 glaciers). Data on measurements on Morteratsch have been provided by J. Oerlemans. Stake measurements from 12 glaciers are from own measurements, conducted during the summer of 2002. Melt measurements on four glaciers during the summer 2003 are from *Zemp et al.* [2005].

[17] The temporal variability of the modeled mass balance is compared to mean annual mass balances of 9 Alpine glaciers (two of them, Silvretta and Gries, being located in Switzerland) [*World Glacier Monitoring Service* (*WGMS*), 2007] and to the results of *Huss et al.* [2008] who applied a combined approach of geodetic mass balance measurements, stake measurements and mass balance modeling to obtain long-term mass balance series of four Swiss glaciers: Silvretta, Great Aletsch, Gries and Rhône (see Figure 1).

4. Computation of the Mass Balance

4.1. Mass Balance Model

[18] The applied glacier mass balance model is a simplified version of more sophisticated energy balance approaches. However, it still includes one of the main features of energy balance models, a separate treatment of shortwave radiation and energy fluxes depending strongly on air temperature (turbulent and longwave fluxes). In particular the calculation of the latter is largely simplified whereas the calculation of shortwave radiation is similar to more complex energy balance approaches [e.g., *Arnold et al.*, 1996].

4.1.1. General Outline

[19] Apart from the DTM and the glacier outlines (section 3.1), the model basically relies on the three meteorological parameters T_a, S_{in} and P. The model runs at daily steps, and the cumulative mass balance b_c on day $t + 1$ is calculated for every time step and over each grid cell of the DTM according to *Oerlemans* [2001],

$$b_c(t+1) = b_c(t) + \begin{cases} \Delta t \cdot (-Q_m)/l_m + P_{\text{solid}} & \text{if } Q_m > 0 \\ P_{\text{solid}} & \text{if } Q_m \le 0, \end{cases} \quad (1)$$

where t is the discrete time variable, Δt is the time step, l_m is the latent heat of fusion of ice (334 kJ kg^{-1}) and P_{solid} is solid precipitation in meter water equivalent (mwe). The energy available for melt (Q_m) is calculated as follows:

$$Q_m = (1 - \alpha)S_{in} + C_0 + C_1 T_a, \quad (2)$$

where α is the albedo of the surface, S_{in} is the global radiation, T_a is the air temperature (in °C at 2 m above ground and outside the glacier boundary layer) and $C_0 + C_1 T_a$ is the sum of the longwave radiation balance and the turbulent exchange linearized around the melting point [*Oerlemans*, 2001]. The variable C_1 is set to 10 W m^{-2} K^{-1} according to the recommendation of *Oerlemans* [2001] while C_0 was used as a tuning factor and adjusted to fit measurements on Morteratsch glacier for the mass balance year 1998/1999 [*Klok and Oerlemans*, 2002], yielding best fit of observed and modeled mass balances at −45 W m^{-2}. In equation (2), T_a actually stands for ΔT which is the difference between T_a and the glacier surface temperature (T_{surf}). In the present model, T_{surf} is fixed to the melting point (0°C) and hence $\Delta T = T_a$. Consequently the modeled energy balance in winter is not zero but often very negative which is obviously wrong. However, according to equation (1), negative Q_m are of no influence to the mass balance.

Assuming $T_{surf} = 0°C$ neglects that the cold content in the winter snowpack needs at first to be removed in spring before melting can take place. Hence a slightly more negative mass balance will result. However, it has been shown by *Greuell and Oerlemans* [1986] that the effect is small for the mostly temperate Alpine glaciers and can be neglected.

4.1.2. Accumulation

[20] In the present mass balance model the source of accumulation is solid precipitation, redistribution of snow by wind or avalanches is not considered (for a model that includes avalanches, see *Machguth et al.* [2006b]). Refreezing is not taken into account and any melt water and rainfall is immediately removed from the glacier. A threshold temperature (T_{snow}) of 1.5°C in combination with a transition range of 0.5°C is used to distinguish snowfall and rain. The resulting gradual transition from snow to rain with 100% snow at $T_a = 1°C$ and 0% snow at $T_a = 2°C$ agrees fairly well with the long-term observations on air temperature and snow-rain transition, compiled by *Rohrer* [1989] for the weather station in Davos (1590 m asl; see Figure 1).

4.1.3. Incoming Solar Radiation

[21] Global radiation (S_{in}) is calculated from potential clear-sky global radiation ($S_{in,clr}$) and cloudiness (n). The latter is acquired from REMO output whereas $S_{in,clr}$ is computed through a radiation code [*Corripio*, 2003]. Though global radiation is directly available from REMO (S_{in}^{REMO}) the approach described in the following seems easier to apply since S_{in}^{REMO} is at 1/6° spatial resolution and does not consider slope and aspect. Furthermore, mean S_{in} obtained from our approach using only cloudiness from REMO and S_{in}^{REMO} yield similar deviations to measured mean S_{in} at the 14 selected weather stations (see Table 2).

[22] $S_{in,clr}$ is computed according to *Corripio* [2003] and *Iqbal* [1983]. $S_{in,clr}$ is the sum of diffuse ($S_{in,clrdif}$) and direct radiation ($S_{in,clrdir}$) which are both calculated separately. For the latter all effects of surface topography including shading are considered. Daily means of both components of $S_{in,clr}$ are obtained from a calculation at a temporal resolution of 30 min. This calculation is only performed once in the preprocessing and the resulting 365 arrays of daily mean $S_{in,clrdif}$ and $S_{in,clrdir}$ for all days of the year are stored (in leap years the arrays of day number 365 are simply used twice). The preprocessing procedure allows for a strong reduction of computation time. However, atmospheric transmission coefficients (such as for Rayleigh scattering, water vapor and other gases, aerosol extinction, etc.) are applied in the preprocessing only for a standard atmospheric composition and cannot be altered later. Only attenuation of clouds (τ_{cl}) is calculated for every individual time step in the actual model run according to a relationship established by *Greuell et al.* [1997] based on measured S_{in} and observed n on the Pasterze glacier in the Austrian Alps,

$$\tau_{cl} = 1.0 - 0.233n - 0.415n^2. \quad (3)$$

[23] Cloudiness varies from 0 (cloud free) to 1 (complete overcast). τ_{cl} is then used to compute S_{in} from $S_{in,clr}$,

$$S_{in} = S_{in,clr}\tau_{cl}, \quad (4)$$

where $S_{in,clr} = S_{in,clrdif} + S_{in,clrdir}$. A lower threshold of $S_{in,clrdif}$ is applied in order to avoid reduction of S_{in} below the value of $S_{in,clrdif}$ on grid cells that receive little or no direct radiation due to shading or exposition: Whenever for a particular grid cell S_{in}, calculated according to equation (4), falls below $S_{in,clrdif}$, then: $S_{in} = S_{in,clrdif}$.

[24] Global radiation calculated according to the above described approach is in the following denoted as $\hat{S}_{in}$ since the calculation is based upon $\hat{n}$ which is interpolated from the REMO output (see section 4.2).

4.1.4. Albedo Parameterization

[25] The ice surface is always treated as debris-free. Depending on whether the surface is composed of snow, firn or ice, three different and fixed values for the surface albedo are used in the model: $\alpha_s = 0.72$, $\alpha_f = 0.45$ or $\alpha_i = 0.27$, respectively. In the test runs for Morteratsch glacier $\alpha_s = 0.72$ was used and resulted in reasonable melt rates for the snow cover. The firn albedo is of rather small influence to the model result while α_i is decisive to the model output. During the test runs, $\alpha_i = 0.34$ was used according to *Klok and Oerlemans* [2002]. However, this value seems rather high to represent a mean for all Swiss glaciers [e.g., *Paul et al.*, 2005] and we apply $\alpha_i = 0.27$ in this study. At the start of the calculation the albedo is set to α_i for the entire glacierized area, and for any snow accumulation α_s is used. Accumulated snow is assigned α_f when its age exceeds 1 year and after 2 years its albedo is lowered to α_i. The idea behind this parameterization is an approximation of the albedo lowering related to the snow to ice conversion. Other aspects of the snow to ice transition are not addressed here. Although the model runs at daily steps, surface albedo is allowed to change somewhere in the middle of a time step if, for instance, the snow or firn cover remaining from the last time step was already very thin or after a small snowfall event.

4.1.5. Limitations of the Mass Balance Model

[26] Simplifications in the model make it impossible to calculate reasonable mass balance values for all types of glaciers. For instance, glaciers are regarded as debris-free and thus mass balance of debris-covered glaciers cannot be modeled accurately. For simplicity, model runs are performed for all glaciers of the Swiss Alps but most of the statistical analysis is performed only for a selection of glaciers where reasonable mass balance calculations are expected. These glaciers are selected manually based upon the following criteria: (1) no or little debris cover, (2) no or little influence of avalanches, (3) mass loss restricted to melting and (4) considerable size (area > 1 km^2). Altogether, 94 glaciers were found to meet these conditions. The selected glaciers cover an area of 610 km^2, or roughly 50% of the total glacierized area.

4.2. Downscaling of the REMO Output

[27] The spatial resolution of the input data (REMO) and the DTM differs greatly and downscaling has to be applied to make the daily fields of REMO output applicable to the mass balance calculation. For this purpose we treat the centers of the REMO boxes as virtual weather stations. All data related to the REMO boxes are assigned to their respective centers. The downscaling procedure includes two steps: (1) the values in between the virtual weather stations are interpolated to the DTM resolution by means of

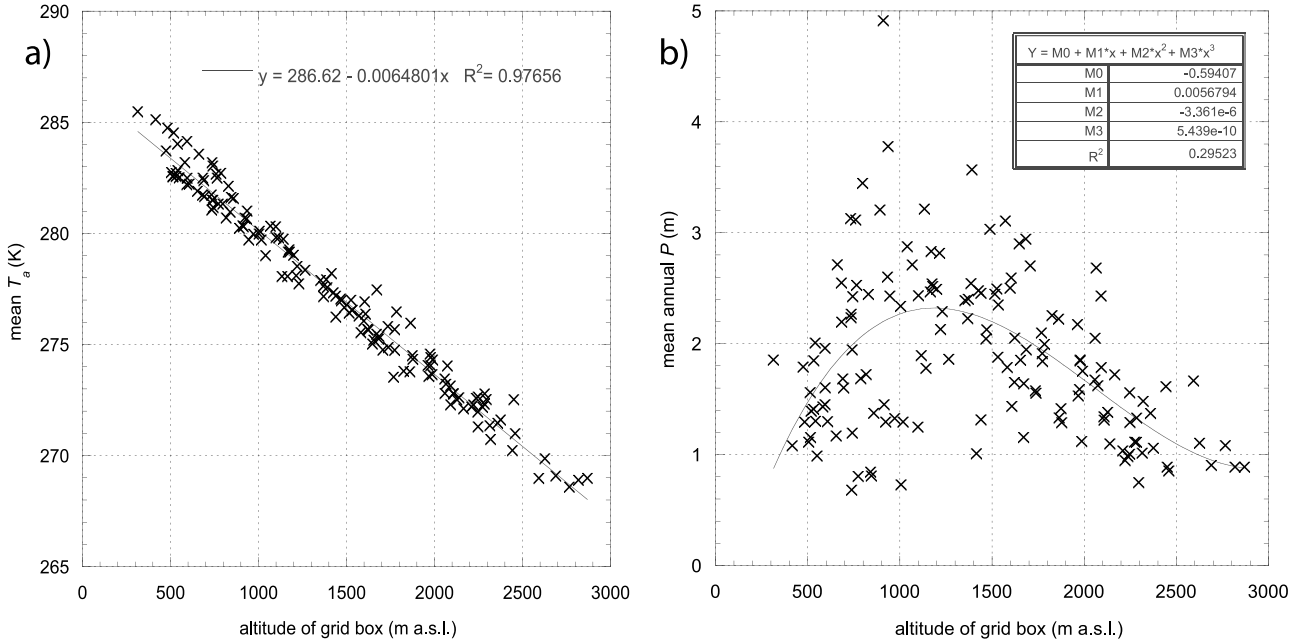

Figure 2. (a) Mean T_a of the time period 1979–2003 for all REMO grid boxes of the Swiss Alps, plotted against grid box elevation. (b) Mean annual P of the time period 1979–2003 for all REMO grid boxes of the Swiss Alps, plotted against grid box elevation (number of grid boxes is 150).

interpolation techniques as described in the following paragraph and (2) parameterizations to account for variability on a subgrid scale are applied.

[28] The results of different interpolation schemes may vary and thus influence mass balance distribution. Consequently, we apply three widely used techniques: The Nearest Neighbor interpolation (NN), Inverse Distance Weighting (IDW) and Thin Plate Splines (TPS). The first was applied because it basically alters only the spatial resolution of the data while preserving the original values: NN results in areas of identical value and location, as well as near-identical shape of the original REMO grid boxes. However, these areas are then composed of 100 m cells. The disadvantage of NN are step changes at the boundaries of the areas representing the original 1/6° grid boxes. On the contrary, IDW and TPS interpolate in between the virtual weather stations by generating new values. IDW interpolates by predicting new values within the range of the original values while TPS may result in new values outside this range [*Burrough and McDonnell*, 2004]. IDW as applied here is an exact interpolator; predicted values at the virtual weather stations are always identical to the original values. Also TPS is an exact interpolator, but within smoothing limits [*Burrough and McDonnell*, 2004]. Both interpolators generate smooth surfaces. Consequently, a prerequisite to their application is that the unknown "real" surface which should be approximated by the interpolation is smooth [*Burrough and McDonnell*, 2004]. Meteorological quantities are not necessarily distributed smoothly in space. However, in our case the interpolation schemes are not used to reproduce an unknown "real" distribution since this is not possible from the RCM output alone. They are applied to generate smooth transitions from one virtual weather station to the next because such a pattern is still more realistic than abrupt breaks from one RCM grid box to the next. The key question is which interpolator performs good in generating smooth surfaces while preserving characteristics of the REMO data, such as meteorological means and wet-day frequency (WET).

[29] Interpolations have been carried out with the "griddata" routine included in the IDL software distribution [*RSI Research Systems Inc.*, 2004]. To allow for a faster computation in "griddata" the maximum number of nodes used for interpolation was reduced to 12 (IDW) and 24 (TPS). A lower threshold for interpolation with TPS resulted in interpolation artifacts. In the following, the term "interpolated" refers to the application of NN, IDW or TPS. For reasons of simplicity, only one interpolation technique is used in the course of a model run.

4.2.1. Downscaling of Air Temperature

[30] Values of T_a strongly depend on the elevation of the respective REMO boxes (Figure 2a). Prior to the interpolation this dependence on altitude has to be removed. The values for T_a at the virtual weather stations are reduced to a standard altitude H_0 = 0 m asl by means of a fixed atmospheric lapse rate (Γ_{Ta}). The selection of an atmospheric lapse rate is a critical issue in mass balance modeling [e.g., *Machguth et al.*, 2008] because of its seasonal and spatial variability. We have chosen $\Gamma_{Ta} = -0.0065$ K m^{-1} according to the slope of the linear regression of grid box altitude and mean annual air temperature in REMO (Figure 2a). The value is derived directly from REMO to avoid inconsistencies of the original REMO data and the downscaled data. The chosen Γ_{Ta} is in good agreement to near surface summer lapse rates in the Alps [*Rolland*, 2003]. Seasonality of the lapse rate is not considered but a good representation of summer air temperatures is achieved which strongly governs mass balance on the temperate Alpine glaciers. Note that the mean lapse rate in REMO is very similar to the international standard atmosphere lapse rate (-0.0065 K m^{-1}). Never-

theless, Γ_{Ta} is not prescribed by the RCM but generated internally by the model physics and dynamics of REMO. The dependence on altitude is eliminated from equation (5),

$$T_a^{\mathrm{red}} = T_a - \mathrm{DTM}_{\mathrm{REMO}} \cdot \Gamma_{Ta}, \tag{5}$$

where T_a^{red} is the reduced air temperature, $\mathrm{DTM}_{\mathrm{REMO}}$ is the REMO topography at native resolution. T_a^{red} is then interpolated to a 100 m array ($\hat{T}_a^{\mathrm{red}}$). The influence of elevation is finally reintroduced, based on the 100 m DTM,

$$\hat{T}_a = \mathrm{DTM} \cdot \Gamma_{Ta} + \hat{T}_a^{\mathrm{red}}, \tag{6}$$

where DTM is the 100 m DTM. Of course a reduction to a standard level is superfluous when using NN but for simplicity all interpolation techniques are treated identically.

4.2.2. Downscaling of Precipitation

[31] Precipitation is a critical parameter due to its high spatial and temporal variability and large uncertainties in the measurements. Furthermore, snow is redistributed by wind and avalanches, leading to complex accumulation patterns on glaciers [e.g., *Machguth et al.*, 2006a; *Plattner et al.*, 2006]. In this study we have not considered the latter effects (see section 4.1.5) but aim at parameterizing the general characteristics of precipitation distribution. Existing high-resolution precipitation climatologies for the Alps [e.g., *Kirchhofer and Sevruk*, 2001, Plate 2.2; *Schwarb et al.*, 2001, Plate 2.6] show a distinct variability on the local scale with higher values on the ridges and dryer valleys. To derive a similar pattern we apply a precipitation gradient (Γ_P) to account for variability on a subgrid scale.

[32] Prior to the downscaling the REMO output is tested for a general bias by comparison of mean annual P at the 14 weather stations to mean annual P of the 18 km REMO grid boxes they are located within. Mean measured annual P is 1.51 m while the REMO mean amounts to 1.8 m. However, measured values are not corrected for systematic undercatch: According to *Sevruk* [1985], monthly correction values for precipitation measurements in the Swiss Alps reach +50% or more during winter and depend strongly on location and topography at the individual stations. A moderate correction of the measured values by 20% (see also the recommendation of a 15% to 30% correction given by *Schwarb et al.* [2001, Plate 2.6] and discussed later in this study) will bring both data sets in agreement and thus there is no indication of a general bias of the REMO precipitation for the model domain.

[33] The selection of an appropriate value for Γ_P is difficult because Γ_P is spatially variable in the Alps [*Sevruk*, 1997; *Schwarb*, 2000] and values are uncertain due to the large errors in the measurements of precipitation. *Sevruk* [1997] assessed the spatial variability of Γ_P in the Swiss Alps and rejected all measurements of P at sites above 2700 m asl because they were considered too uncertain. Furthermore, horizontal and vertical variability of P cannot be completely distinguished [*Schwarb*, 2000]. An attempt to derive Γ_P from the REMO data, similar to the temperature lapse rate, yields no applicable results: Between 400 and 1000 m asl, P increases with elevation whereas above 1500 m asl the trend is negative (Figure 2b). This picture has three reasons.

[34] 1. The RCM systematically dislocates precipitation from ridges to the foreland, causing a moderate negative precipitation bias at high-elevation sites and a strong positive bias at medium altitudes [*Kotlarski et al.*, 2009].

[35] 2. The REMO model domain contains the dry inner-alpine region with low precipitation at high altitudes. In the spatial mean, this contributes to the reversed precipitation-altitude gradient as derived from the RCM.

[36] 3. At the spatial resolution of REMO the variability of P on a horizontal scale is a major component of total variability among the grid boxes.

[37] For Γ_P we finally applied the value used by *Kirchhofer and Sevruk* [2001, Plate 2.2] for their precipitation map of Switzerland (Γ_P = 0.0008 m yr^{-1} m^{-1}). The idea of using locally variable Γ_P as provided by *Schwarb* [2000] or *Sevruk* [1997] was put aside for reasons of simplicity.

[38] Since Γ_P is given in m yr^{-1} m^{-1}, but has to be applied to daily precipitation sums, it is converted to a dimensionless precipitation correction array ($\hat{\Gamma}_P^*$). This is done prior to the model run, based on *DTM*, the mean annual precipitation for the calculation period ($\hat{P}_{\mathrm{mean}}$) and the REMO topography ($\widehat{\mathrm{DTM}}_{\mathrm{REMO}}$). The latter two variables are interpolated to a 100 m array from P and elevation at the virtual weather stations,

$$\hat{\Gamma}_P^* = \frac{\hat{P}_{\mathrm{mean}} + \left(\left(\mathrm{DTM} - \widehat{\mathrm{DTM}}_{\mathrm{REMO}}\right) \cdot \Gamma_P\right)}{\hat{P}_{\mathrm{mean}}}. \tag{7}$$

[39] In the model run, precipitation distribution at a specific date is then calculated to $\hat{P} = \hat{P}_d\, \hat{\Gamma}_P^*$, where $\hat{P}_d$ is the precipitation sum of the current day interpolated from the virtual weather stations to a 100 m grid. A reduction of P to a standard level prior to the interpolation could even exaggerate the systematic biases inherent to the REMO data and is thus not performed. Negative $\hat{P}$ values that may occur when using TPS are set to zero.

[40] For illustration, the interpolation and downscaling scheme is applied to mean annual P (Figure 3a), resulting in mean annual $\hat{P}$ as depicted in Figure 3b.

4.2.3. Downscaling of Cloudiness

[41] Mean cloudiness (1979–2003) for the individual REMO grid boxes reveals only a weak positive correlation with elevation (yielding R^2 = 0.17 in a linear regression). Consequently, cloudiness is interpolated directly from the virtual weather stations to a 100 m array ($\hat{n}$) and an altitudinal gradient is not applied. Attenuation of clouds is then calculated from interpolated cloudiness and applied to obtain $\hat{S}_{in}$ (see section 4.1.3).

4.3. Implementation

[42] A flow chart of the processing steps is given in Figure 4. The structure is optimized to keep computation time short because the calculation of solar radiation (section 4.1.3) and the three daily interpolations of the REMO data (see section 4.2) are time consuming.

[43] The calculation of clear-sky global radiation is conducted in the course of the preprocessing and on the full DTM in order to allow for the computation of shading. From the resulting arrays of $S_{\mathrm{in,clrdif}}$ and $S_{\mathrm{in,clrdir}}$ the values for the glacierized cells are extracted and converted into a

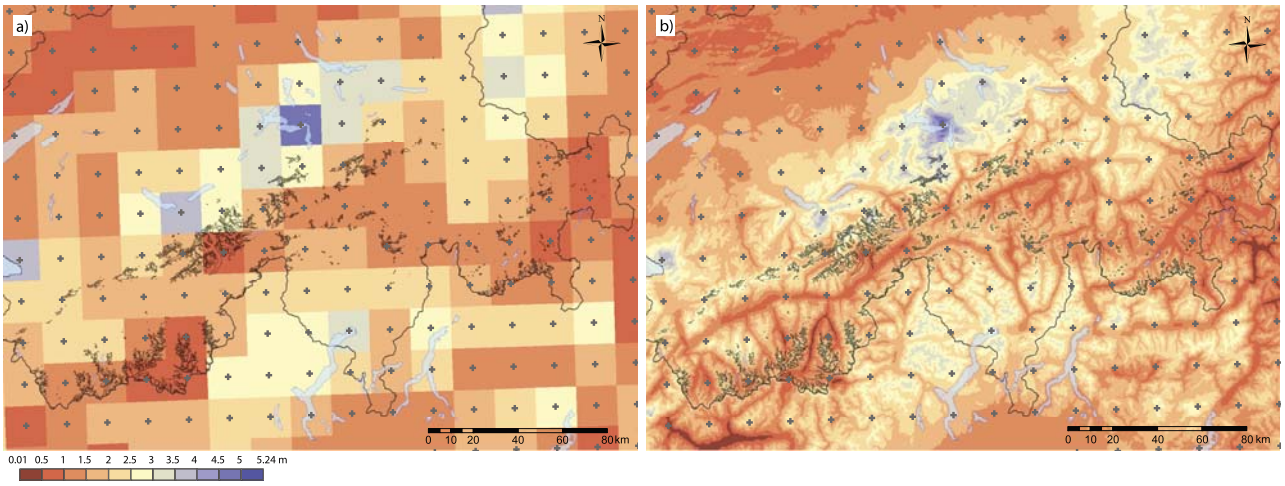

Figure 3. (a) Mean annual P over the temporal and spatial model domain at the native REMO resolution. (b) Mean annual $\hat{P}$ after interpolation with IDW and application of the altitudinal gradient. For orientation, the border of Switzerland is shown in black, glacier outlines are gray, and lakes are light blue. The floating point values in the legend (0.01 and 5.24) indicate the absolute minimum and maximum of the displayed data. Note that the maximum value in Figure 3a is 4.9 m yr^{-1} and no other grid box exceeds 3.8 m yr^{-1} (see Figure 2b).

simple one dimensional columnar format. Furthermore, the DTMs glacierized cells are also transferred into columnar format. These files are then used for input in the actual model run. Hence, the mass balance calculation and the related interpolations of the REMO data are performed only for the glacier surfaces of the Swiss Alps.

[44] During the model run the measured data at the selected weather stations are consecutively compared to interpolated REMO data at the respective grid cells. In order to compare values of S_{in} being measured normal to a horizontal surface, the DTM is set to equal altitude over 3 × 3 matrices at the locations of the stations prior to the radiation calculation. For the comparison to the measurements, we then use the horizontal central cells of the 3 × 3 matrices.

[45] The individual stake measurements are compared to modeled mass balance at the corresponding grid cell whenever an observation date is encountered.

[46] The final output includes the comparison of measured meteorological parameters to $\hat{T}_a$, $\hat{P}$ and $\hat{S}_{in}$, of measured and modeled mass balance at individual stakes as well as modeled winter, summer and annual balances for the 94 selected glaciers and the 24 mass balance years. The final cumulative mass balance distribution is written to an array and division by the number of mass balance years (24) yields mean annual mass balance distribution.

5. Results

[47] The presentation of modeled mass balances (section 5.1) and the comparison of meteorological parameters (section 5.2.3) are accompanied by a comparison of mean values for all three interpolation schemes. Figures and maps are based upon REMO data interpolated from IDW. The comparison of temporal variability (section 5.2.1) and stake measurements (section 5.2.2) is restricted to mass balances modeled from IDW.

5.1. Modeled Mass Balance Distribution

[48] Two example maps of the resulting mean annual mass balance distribution over the modeled time period are given: The region around Great Aletsch glacier (Figure 5) and the southeastern part of Valais (Figure S1 in the auxiliary material).[1] Glacier specific mean annual mass balances for all 94 selected glaciers are depicted in Figure 6. In total, 23 glaciers have positive and 71 glaciers negative balances.

[49] A visual assessment of Figure 5, auxiliary material Figure S1 and Figure 6 exhibits regional features: Positive balances are dominant at the entire northern edge of the Swiss Alps while more negative balances are dominating in the east. For the remaining regions mass balances are predominantly negative with adjacent glaciers showing often similar values. Mean mass balances around Zermatt reach from extremely negative (−2.87 mwe) to very positive (0.7 mwe) values. However, around Zermatt some spatial correlation can be found as well with predominantly negative values to the south and positive values to the east.

[50] The modeled equilibrium line (EL) is mostly located on the glaciers, dividing them in an accumulation and an ablation area. The equilibrium line altitude (ELA) resulting from the model run is generally lower at the northern edge, reaching down to 2600–2700 m asl for some glaciers while around Zermatt ELAs culminate at 3200–3400 m asl.

[51] Mean modeled mass balance for all glacierized DTM-cells varies with the interpolator (see Table 1). NN and TPS yield similar results (−1.08 mwe and −1.21 mwe, respectively) while IDW results in a less negative mean of −0.79 mwe. The values do only shift slightly when the mean mass balance is obtained only from cells of the 94 selected glaciers: −1.11 mwe (NN), −1.21 mwe (TPS) and −0.76 mwe (IDW). Subtracting IDW from TPS yields a differential array of lower standard deviation than NN–

[1] Auxiliary materials are available with the full article: doi:10.1029/2009JD011775.

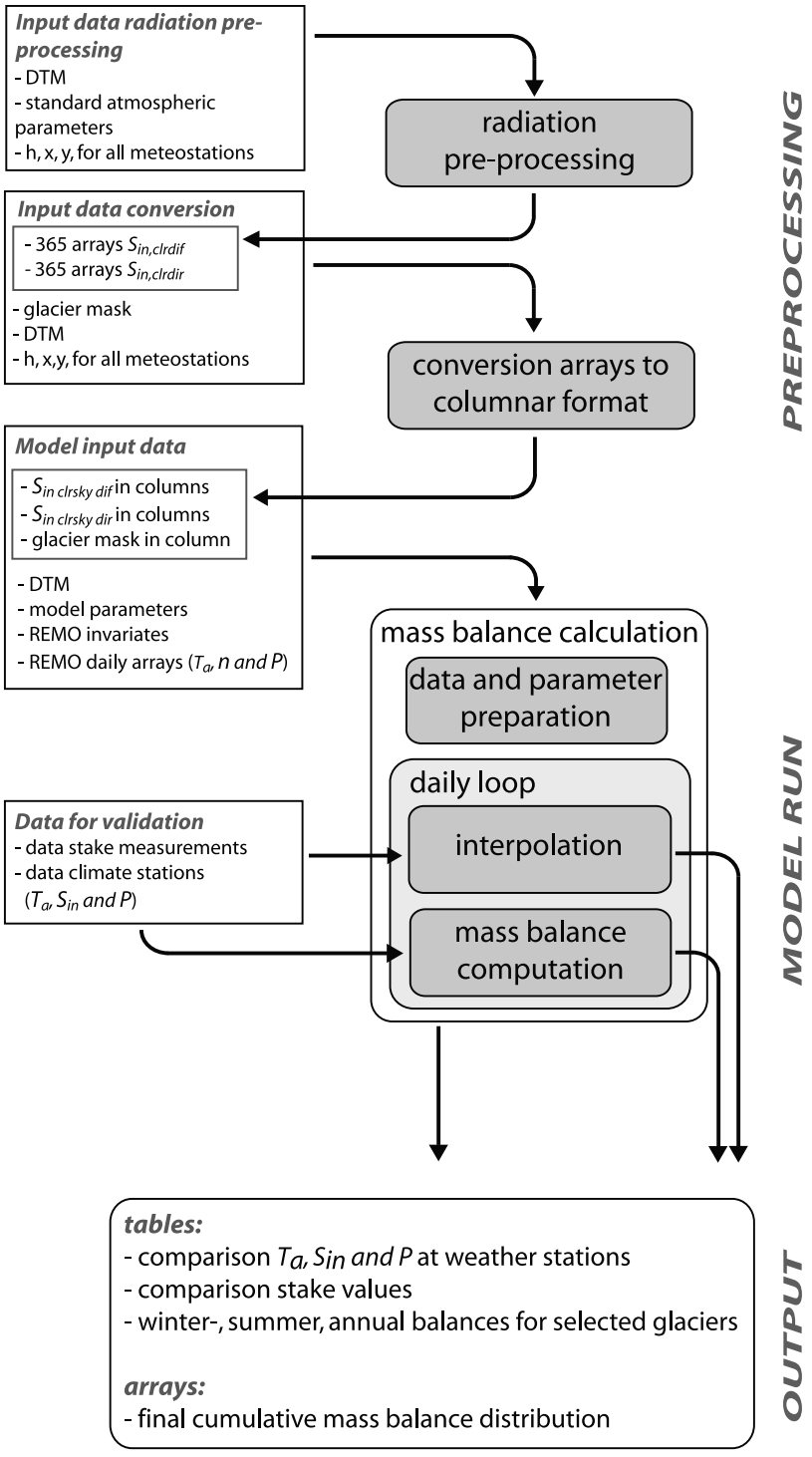

Figure 4. Flowchart of the model structure and the main input and output components.

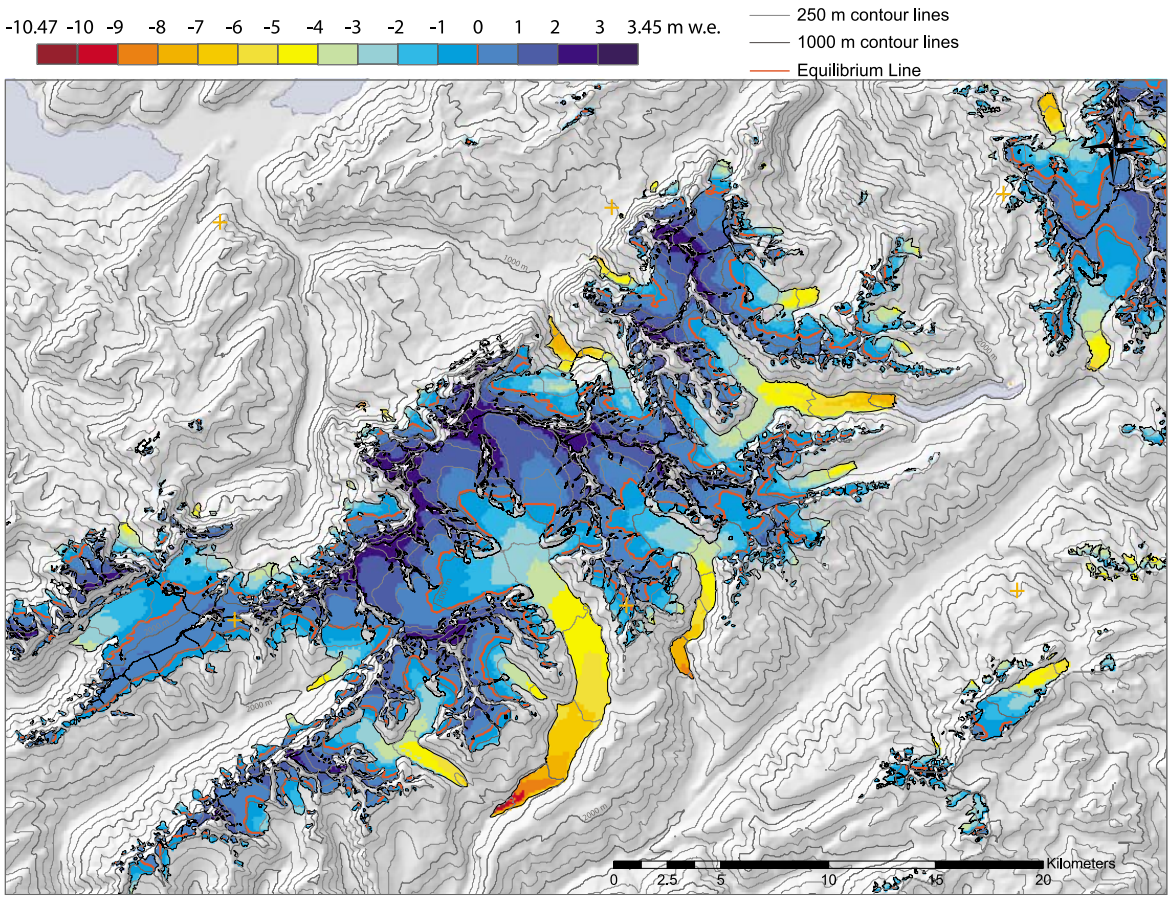

Figure 5. Mean modeled annual mass balance distribution for all glaciers of the region around Great Aletsch glacier (~8°5′E–8°26′E and 46°21′N–46°28′N). The floating point values in the legend (−10.47 and 3.45 mwe) indicate the absolute minimum and maximum of the modeled mass balance for all Swiss glaciers. The minimum of −10.47 mwe is modeled for the tongue of Great Aletsch glacier, and the maximum occurs close to the northern reaches of the same glaciers accumulation area.

IDW or NN–TPS (Table 1), indicating that the spatial patterns of mass balance distribution are more similar between IDW and TPS than compared to NN. Since the former two interpolators generate smooth surfaces their lower standard deviation at pixel resolution was to be expected.

5.2. Validation

5.2.1. Modeled Mass Balance and Annual Variability

[52] The data from *Huss et al.* [2008] are compared to the modeled temporal variability of annual, winter and summer balance on the four glaciers investigated *Huss et al.* [2008] (Figure 7a). Annually averaged balances for the 94 selected glaciers are compared to the data from *Huss et al.* [2008] and from *WGMS* [2007] in Figure 7b. Annual balances from Figure 7a are depicted as well to allow for a direct comparison. It becomes obvious that the curve built from the mean of the 94 glaciers agrees well with the *Huss et al.* [2008] and *WGMS* [2007] data whereas the curve built from the mean of the four glacier sample is systematically lower by ~0.25 to 0.75 mwe. The temporal variability of both samples are similar. Additionally, modeled annual, summer and winter balance are compared in a scatter plot (Figure S2a in the auxiliary material). A linear regression of the annually averaged balance for the 94 glaciers against the *WGMS* [2007] data yields R^2 = 0.82. The data from *Huss et al.* [2008] agree somewhat better with the *WGMS* [2007] data (R^2 = 0.89) while the slope of both regressions is similar (1.12 and 1.09, respectively) (see Figure S2b in the auxiliary material for a visualization of the linear regressions).

5.2.2. Stake Readings

[53] Stake readings used for model validation have been divided into three subgroups and are depicted individually: (1) Stake measurements that are conducted during summer and thus are mainly restricted to melt are compared to modeled values in Figure 8a. (2) On Claridenfirn both winter and annual balances are available and the data are compared in Figure 8b. (3) Data from stakes that are visited only once at the end of a balance year, representing the sum of accumulation and ablation processes are shown in Figure 8c. All modeled values are obtained from the IDW interpolation.

[54] Values in Figure 8a are close to identity with the exception of seven outliers where the model strongly underestimates summer melt (see discussion in section 6.1). All measurements depicted in Figures 8b and 9c are systematically underestimated by the model. The shift toward more negative modeled mass balances is most pronounced for Silvretta and Gries glacier.

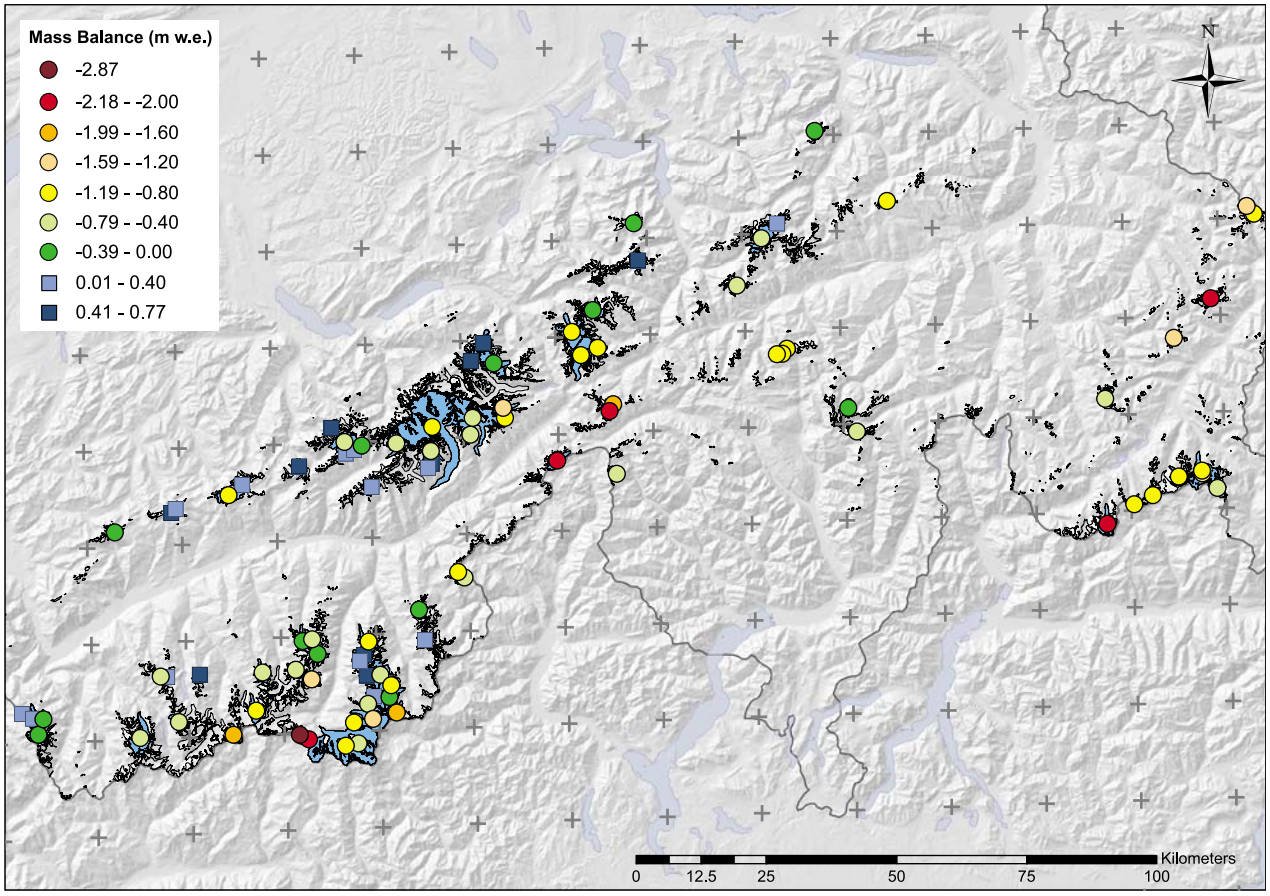

Figure 6. Mean annual mass balances over the calculation period for the 94 selected glaciers. Circles denote negative and squares denote positive mean balances. Glaciers that have not been selected are depicted by hollow glacier outlines.

5.2.3. Modeled Meteorological Parameters

[55] A comparison of measured T_a, P and S_{in} averaged over all 14 weather stations with $\hat{T}_a$, $\hat{P}$ and $\hat{S}_{\text{in}}$, averaged over the DTM cells corresponding to the location of the weather stations for all three interpolators is given in Table 2. Global radiation provided by REMO ($S_{\text{in}}^{\text{REMO}}$) was not used in this study but is compared to the measurements as well in order to compare bias in $\hat{S}_{\text{in}}$ and $S_{\text{in}}^{\text{REMO}}$. Furthermore, $\hat{T}_a$, $\hat{P}$ and $\hat{S}_{in}$ averaged over the entire glacierized perimeter are shown. Wet-day frequency (WET) averaged over the 14 stations and over the corresponding grid cells is shown in Table 2 as well and is here defined as the percentage of days with precipitation >0.1 mm. For the glacierized area we also compare mean annual precipitation of the downscaled REMO fields to mean annual precipitation 1971–1990 of the *Schwarb et al.* [2001, Plate 2.6] precipitation climatology. The 2 km resolution precipitation map has been derived from uncorrected station records and must be corrected for undercatch by 15–30% for areas above 1500 m asl [*Schwarb et al.*, 2001, Plate 2.6]. The values given in Table 2 are corrected uniformly by 15% and 30%. Note that the timeframe of the precipitation data differs: 1971–1990 for *Schwarb et al.* [2001, Plate 2.6] and 1979–2003 for the downscaled REMO precipitation. Mean annual precipitation 1971–1990 of the downscaled REMO fields is 5% larger than for 1979–2003.

[56] There is a cold bias in T_a that only slightly depends on the interpolation scheme. Mean measured values of S_{in} and P are overestimated and the amount of the overestimation varies with the chosen interpolator. The values of $\hat{P}$ and $\hat{S}_{\text{in}}$ obtained from TPS are closest to the observations at the weather stations, IDW introduces the largest bias. Differences among the interpolation schemes are most pronounced for precipitation: when TPS is applied to calculate $\hat{P}$, precipitation over the glacier perimeter is reduced by 16% compared to IDW. While the comparison to observations at the weather stations indicates an overestimation of P, mean precipitation over the glacier perimeter is in reasonable agreement with *Schwarb et al.* [2001, Plate 2.6] when using IDW. The application of NN and TPS results in an underestimation. The agreement becomes even better when comparing the *Schwarb et al.* [2001, Plate 2.6] data to $\hat{P}$ for the 1971–1990 time period because REMO precipitation was higher then by 5%. Wet-day frequency is clearly higher when using IDW

Table 1. Comparison of Mean Mass Balances Computed With the Three Interpolation Schemes and the Related Standard Deviations

	All Glaciers	Selected Glaciers
NN - IDW	−0.27 ± 0.58	−0.35 ± 0.53
NN - TPS	0.14 ± 0.63	0.10 ± 0.60
IDW - TPS	0.41 ± 0.38	0.45 ± 0.37

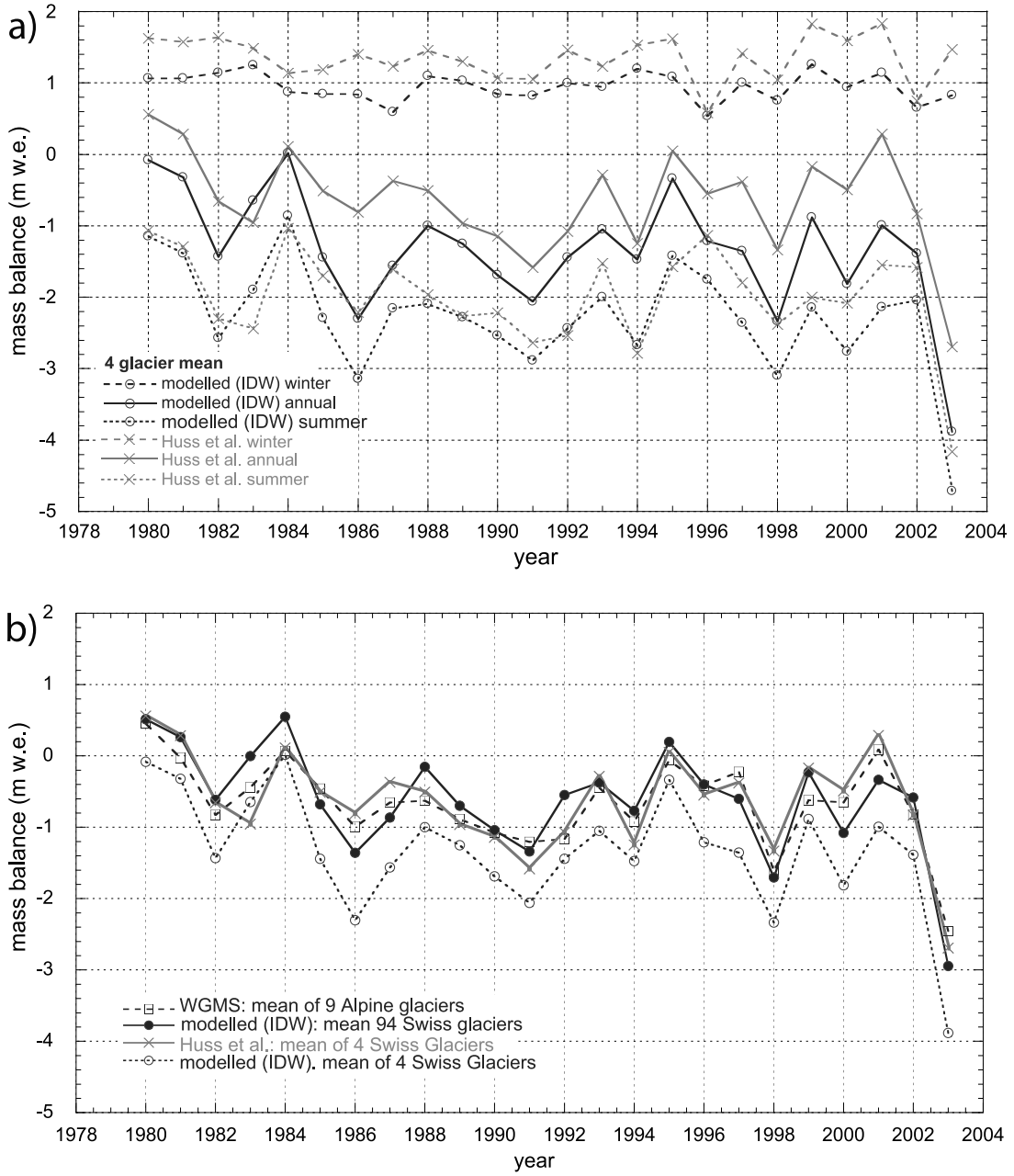

Figure 7. (a) Modeled winter, summer, and annual balances over the calculation period compared to the values from *Huss et al.* [2008]. Values are the mean of the four glaciers: Great Aletsch, Gries, Rhône, and Silvretta. (b) Annual mean mass balances for the 94 selected glaciers compared to annual means from *Huss et al.* [2008] and *WGMS* [2007]. To allow for a direct comparison to Figure 7a, modeled mean annual balance for the four glaciers sample size is depicted as well.

while both NN and TPS are in close agreement to the observations. While $S_{\text{in}}^{\text{REMO}}$ underestimates measured S_{in} by 13 W m^{-2} (on average), our approach overestimates the observations by 9 (TPS) up to 16 W m^{-2} (IDW).

[57] Mean measured T_a, P and S_{in} at the individual weather stations are compared to mean $\hat{T}_a$, $\hat{P}$ and $\hat{S}_{\text{in}}$ at the respective DTM cells in three scatter plots (Figures 9a, 9b and 9c). Mean values are calculated over the number of days with available data at the respective stations. Air temperature correlates best, a weak correlation can be established between P and $\hat{P}$ while no correlation exists for global radiation. In correspondence with Table 2, T_a is underestimated by $\hat{T}_a$ while the other two parameters are overestimated at most stations.

6. Interpretation

[58] In the following, the modeled mass balance distribution is analyzed in relation to the comparison of stake measurements and the temporal variability of mass balance. Special emphasis is laid on effects of the different interpolators. Finally, the comparison of meteorological data is examined.

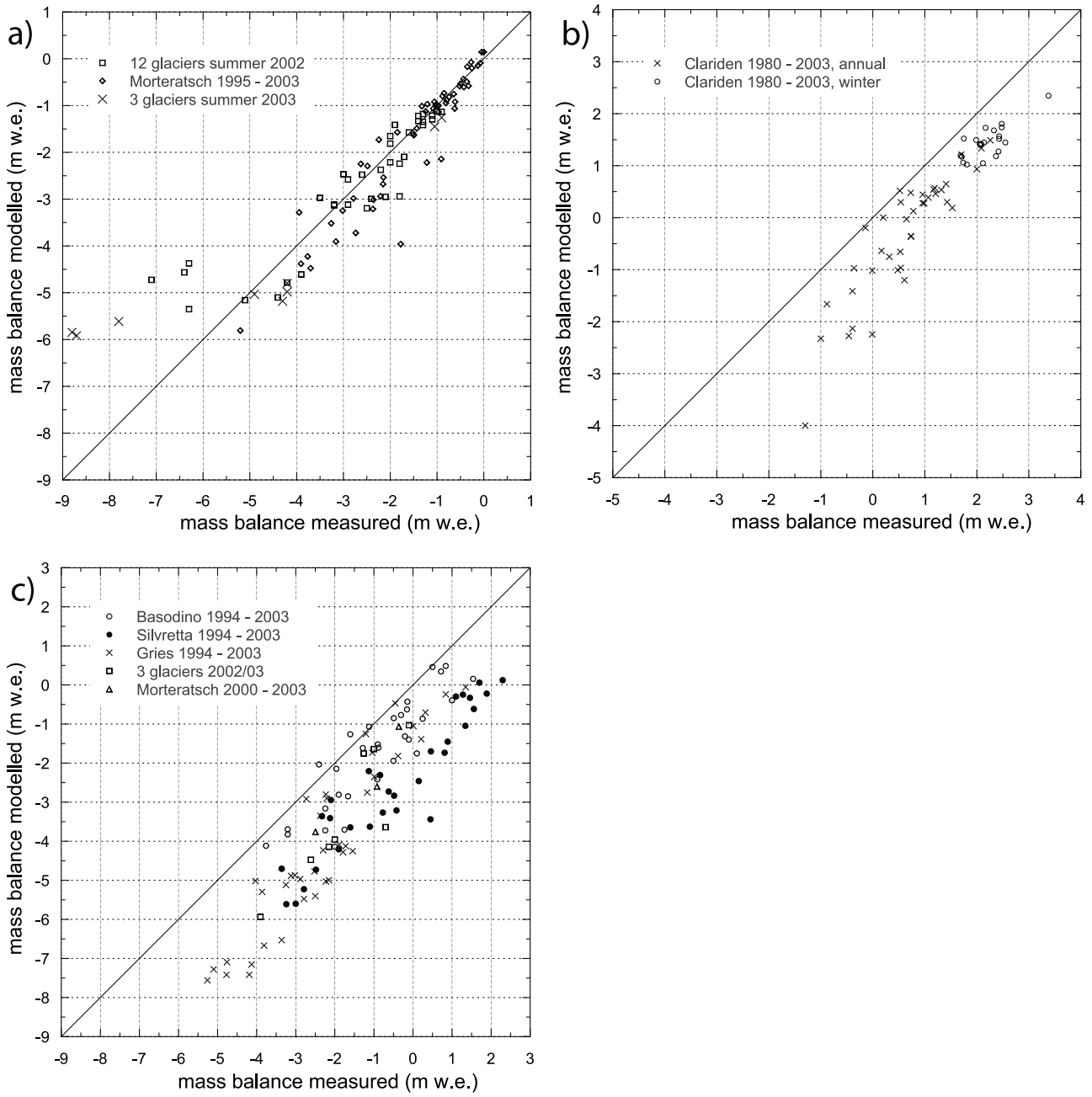

Figure 8. Scatterplot of observed and modeled mass balances at stake locations. (a) Comparisons for stake readings of summer balances, dominated by melt processes. (b) Readings from Claridenfirn where winter and annual balances are available. (c) Stake readings that refer to a full balance year and thus incorporate both accumulation and ablation.

6.1. Calculated Mass Balance

[59] An assessment of the quality of the modeled mass balance distribution is rather difficult because data are available only for a few glaciers. However, a rough assessment can be made by checking visually if the pattern of modeled mass balance agrees with known features: The observed general pattern of low ELAs at the northern edge of the Alps and highest ELAs in the region north of Zermatt [e.g., *Maisch et al.*, 2000] is reproduced well. Furthermore, modeled ELAs are even present on most of the small glaciers with a rather limited extent in altitude, which can be rated a success. On the other hand, the general retreat of all observed glaciers in Switzerland during the modeled time span [*Paul et al.*, 2004] indicates that modeled positive mass balances must be considered unrealistic. There are also areas where modeled mass balances are clearly too negative: for instance, Gries glacier (the largest glacier in the southeastern corner of Figure 5).

[60] Figure 8a indicates that melt is modeled quite well for different types of glaciers spread over a large portion of the Swiss Alps. The seven outliers concern stake measurements on the terminus of Upper Grindelwald glacier, situated in a very narrow and deep gorge that cannot be

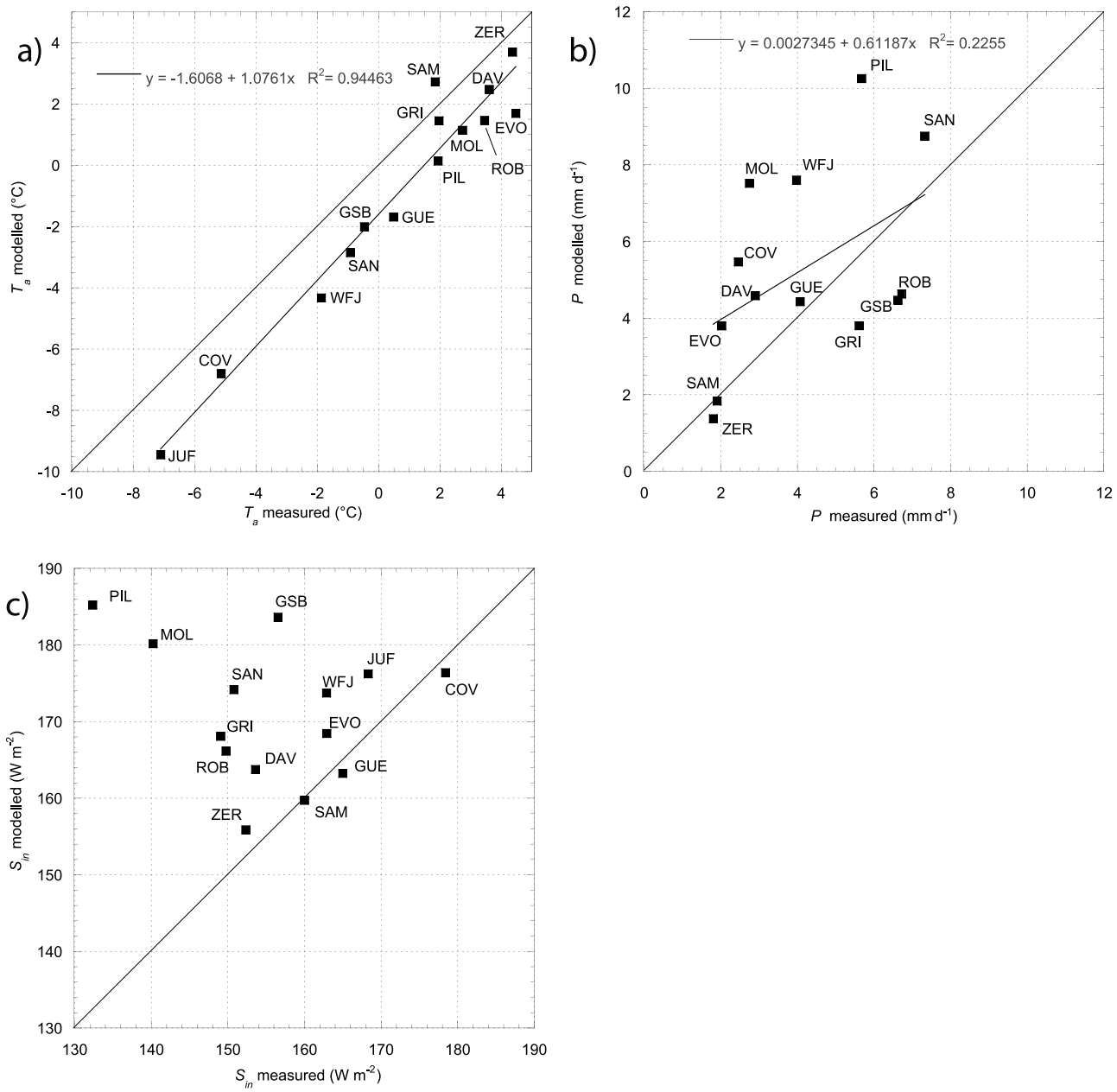

Figure 9. Mean interpolated and downscaled values of (a) T_a, (b) P, and (c) S_{in} are plotted against observed means at the 14 selected weather stations of MeteoSwiss. For every individual station, mean values are calculated over the time span where measured data are available.

resolved by the 100 m DTM. Warm air currents and modification of the longwave radiation balance due to the surrounding rock walls are also possible reasons for the systematic underestimations of melt on that glaciers terminus. Since melt for all other glaciers is modeled well, the systematic underestimation of annual and winter balances (Figures 8b and 8c) is attributed to an underestimation of accumulation. This assumption is confirmed by the systematic underestimation of winter balance on Claridenfirn (Figure 8b).

[61] The assumption of a systematic underestimation in accumulation is also supported by Figure 7a: Underestimations are persistent in winter balances. Although less pronounced, summer balances are also underestimated which might be caused by the albedo feedback mechanism related to reduced snow cover at the end of the winter and underestimations of summer snowfall. Figure 7b indicates that such underestimations might be a local effect which tends to average out when a larger sample is considered. Indeed, annual variability and the mean of modeled mass balances for the 94 glacier sample are very similar to the data from *WGMS* [2007] and *Huss et al.* [2008] while the curve for the small sample is clearly shifted toward more negative values.

[62] The mass balance model contains simplifications. Still, modeled and measured melt agree quite well for a large number of glaciers indicating that the simplifications (e.g., α_i is constant throughout the entire model domain) do not impact much on melt modeling, compared to the

Table 2. Comparison of Measured and Modeled Meteorological Parameters Obtained From the Three Interpolation Schemes[a]

		Weather Stations		Glacier Perimeter	
Parameter	Interpolation	Measured	Modeled	Measured	Modeled
T_a (°C)	NN		−0.81		−5.79
	IDW	0.67	−0.88		−5.73
	TPS		−0.74		−5.69
P (mm d^{-1})	NN		5.1		5.0
	IDW	4.1	5.3	5.7 to 6.4	5.7
	TPS		4.5		4.8
WET	NN		52%		
	IDW	49%	63%		
	TPS		51%		
S_{in} (W m^{-2})	NN		168		139
	IDW	156	172		145
	TPS		165		138
S_{in}^{REMO} (W m^{-2})	NN	156	143		

[a]Wet-day frequency (WET) is given as the percentage of days with $P > 0.1$ mm or $\hat{P} > 0.1$ mm. Measured P over the glacier perimeter is according to *Schwarb et al.* [2001, Plate 2.6]. The values are corrected by 15% (5.7 mm d^{-1}) and 30% (6.4 mm d^{-1}). Note that all measured values do not depend on the interpolators.

influence of RCM biases. Furthermore, glacier surfaces and outlines are fixed and an adaption of glacier geometry as a reaction to mass imbalance through retreat or advance, as well as related feedback processes, cannot take place. In Figure 7a differences in annual mass balance seem to be larger in more recent years. However, in 1999, 2000 and 2001, the differences are mainly due to underestimations of the winter balance which cannot be attributed to changing glacier geometry. The impact of such simplifications is not investigated here and could become large when the model is applied to longer time spans [*Huss et al.*, 2008].

6.2. Role of the Different Interpolators

[63] The main reason for the less negative mass balances obtained from IDW are spatial autocorrelations of the location of glaciers and REMO parameters. The effect is most pronounced with P (Table 2).

[64] As depicted schematically in Figure 10, positive and negative differences between the REMO topography interpolated with IDW ($\widehat{\mathrm{DTM}}_{\mathrm{IDW}}$) and NN ($\widehat{\mathrm{DTM}}_{\mathrm{NN}}$) (note that subscript $_{\mathrm{REMO}}$ is omitted for simplicity) occur. Over the full spatial model domain, these differences average each other out and the mean altitude of $\widehat{\mathrm{DTM}}_{\mathrm{IDW}}$ and $\widehat{\mathrm{DTM}}_{\mathrm{NN}}$ varies by only 2 m. However, glaciers are not equally distributed over the terrain but preferentially exist where both the real topography and the REMO grid boxes are highest. Hence, their occurrence is spatially autocorrelated to areas where the $\widehat{\mathrm{DTM}}_{\mathrm{IDW}}$ surface is located below $\widehat{\mathrm{DTM}}_{\mathrm{NN}}$ (Figure 10). When considering only the glacierized area, $\widehat{\mathrm{DTM}}_{\mathrm{IDW}}$ is by average 181 m lower than $\widehat{\mathrm{DTM}}_{\mathrm{NN}}$. As $\Delta_{\mathrm{DTM}} = \mathrm{DTM} - \widehat{\mathrm{DTM}}_{\mathrm{REMO}}$ is applied in equation (7) and because IDW results in a higher mean Δ_{DTM}, increased precipitation is obtained compared to NN.

[65] No overestimation of $\hat{P}$ compared to NN results from TPS (Table 2) although the approach is the same as described above. In contrast to IDW, TPS gives interpolated values that may lie outside the range of original values and thus the peaks in the interpolated REMO topography lie above the elevation of the REMO grid cells, resulting in $\widehat{\mathrm{DTM}}_{\mathrm{TPS}} - \widehat{\mathrm{DTM}}_{\mathrm{NN}} = 25$ m for the glacier perimeter.

[66] Furthermore, the different characteristics of NN, IDW and TPS also affect wet-day frequencies (WET). While NN preserves the original WET of the REMO data, TPS is conservative with respect to the original value. The IDW interpolation results from calculating the distance weighted mean of all nodes within a search radius around the interpolant. When only one node within the search radius has significant precipitation the interpolant will be assigned a value above zero. The larger WET from IDW does not alter mean $\hat{P}$ but rather results in a smoother precipitation distribution with smaller $\hat{P}$ over a large perimeter instead of larger $\hat{P}$ on a smaller area. In the present model, enhanced WET is without influence to the results because α_s is a fixed value and surface albedo can switch even in the middle of a time step (see section 4.1.4). However, more detailed mass balance models contain parameterizations of snow surface aging [e.g., *Klok and Oerlemans*, 2002] and frequent small snowfalls will suppress the aging process.

[67] Air temperature is reduced to a standard level prior to the interpolation and thus the correlation of glacier surfaces with areas of coldest air temperatures is removed.

[68] The slightly higher $\hat{S}_{in}$ computed from IDW can only be due to different mean $\hat{n}$. Similar to the interpolation of the REMO topography, a spatial correlation of the glacier distribution and $\hat{n}$ causes the shift. However, the correlation is less pronounced here and the effect is small.

[69] How can such effects be reduced or avoided? An interpolation scheme is required which preserves the mean over the entire interpolation area and over the area of every REMO grid box. The Nearest Neighbor interpolation meets these requirements. Despite its disadvantage of creating breaks at the borders of the RCMs grid cells, NN is probably the interpolation scheme of choice if the aim is to calculate mean mass balances for entire mountain ranges. On the other hand, a study focusing on the mass balance distribution in detail requires the application of IDW, TPS or similar interpolation schemes to generate smooth transitions.

6.3. Comparison to Meteorological Data

[70] The topography of the Alps is highly complex, resulting in many local climatic effects [e.g., *Schär et al.*, 1998]. The REMO output at 1/6° spatial resolution and also

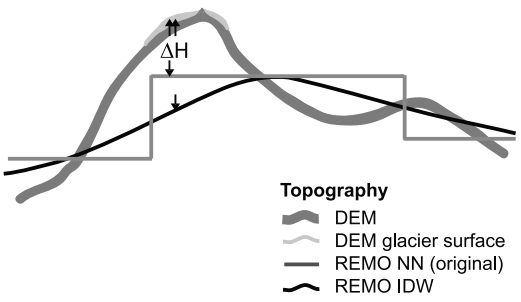

Figure 10. A schematic illustration of how the correlation between the spatial location of glaciers and the highest REMO grid boxes systematically influences ΔH.

after downscaling is, of course, not able to reproduce such small-scale effects. However, comparing the downscaled REMO output to measurements at point locations (Figure 9) is performed for two reasons: (1) If the sample of point measurements is large enough, local effects at the individual stations should average out and an estimate on general biases in the downscaled REMO output can be derived. (2) The variability of the observations around the mean value or around some general trend (e.g., temperature lapse rate) provides information on how large local variability is.

[71] While general biases can be reduced in future studies by implementing bias corrections, climate models will most likely not be able to successfully reproduce small-scale variability, at least for the next several years. Thus, estimates on small-scale effects helps to determine a general level of uncertainty in mass balance modeling. This can be done, for instance, by means of a parametric uncertainty analysis [cf. *Machguth et al.*, 2008].

[72] Over the glacierized area mean precipitation of the REMO fields downscaled using IDW is in reasonable agreement with the corrected mean annual precipitation according to *Schwarb et al.* [2001, Plate 2.6]. Using NN or TPS results in a good agreement to the uncorrected mean (4.9 mm d^{-1}) and indicates an underestimation with respect to the corrected data. In contrary to these findings, the comparison to P measured at the stations indicates overestimations for all three interpolators (see Figure 9 and Table 2). However, measured P at the stations are not corrected. If we also correct the mean P of all stations by 15% to 30% the value becomes very similar to the downscaled REMO fields. A clear statement if the "correct" amount of precipitation was used for the mass balance calculation is almost impossible to make. At least it can be concluded that mean annual precipitation according to the downscaled REMO fields is within the large bounds of uncertainties which are inherent to measurements at the elevation of glaciers. Then again it is obvious that strong local biases in the downscaled REMO fields exist: Only a weak correlation between $\hat{P}$ and measured P at the individual stations exists (Figure 9b). It is assumed that the large scatter is a combined effect of uncertainties in the measurements and local RCM biases.

[73] A correlation between measured S_{in} and $\hat{S}_{\text{in}}$ cannot be established (Figure 9) and the latter exceed measurements by 16 W m^{-2} on average (IDW), for NN and TPS the positive differences are smaller (Table 2). The most apparent overestimations concern stations located at the northern edge of the Alps. In this region REMO strongly overestimates measured P [*Kotlarski et al.*, 2009] while $\hat{n}$ is even lower than in the central parts of the Alps. This could be due to the large contribution of convective precipitation as generated by the RCM's convection scheme in this region. The associated subgrid cloud systems do not contribute to the mean grid box cloud cover. Furthermore, n is a diagnostic quantity which is computed from the cloud cover in the individual model levels assuming certain overlap characteristics and can therefore be associated with a comparatively large uncertainty. Two other stations with strong overestimations (Grand-Saint-Bernard and Grimsel-Hospiz) are located on passes where local clouds tend to form frequently. Such local effects as well as the stations located at the northern edge of the Alps are not representative for the glacierized area. For the remaining stations, the correlation is better and the overestimation is less pronounced or even close to zero when $\hat{n}$ was obtained from NN or TPS.

[74] The good correlation for air temperature can be expected since this parameter strongly depends on altitude. The shift of the regression line toward colder $\hat{T}_a$ is due to a systematic underestimation of winter temperatures by REMO. Summer temperatures, in contrary, are reproduced well [*Kotlarski et al.*, 2009]. Measured T_a over the Swiss Alps tend to decrease from west to east and more pronounced, from the south to the north [*Schär et al.*, 1998]. It seems that horizontal gradients are reproduced to some degree by REMO: For instance, $\hat{T}_a$ is lower at Säntis (northeastern Switzerland) than on Grand-Saint-Bernard (southwestern Switzerland) although the stations are located at the same altitude. The same is the case for Davos and Zermatt, as well as for Molèson and Robiei climate stations.

[75] Our comparison to measured meteorological conditions also shows that bias in $\hat{S}_{\text{in}}$ and S_{in}^{REMO} are similar although with different signs. The question can be asked if our approach of calculating (S_{in}) using only n from REMO and acquiring other variables (T_a, P) more directly from REMO introduces inconsistencies. On the one hand, a certain level of consistency is given because we use n from REMO which plays an important role in the RCM to calculate $S_{\text{in}}^{\text{REMO}}$. On the other hand, there are numerous sources of possible inconsistencies (e.g., the RCM itself, the interpolation schemes as shown in section 6.2) and we believe that the comparison of $\hat{T}_a$, $\hat{P}$ and $\hat{S}_{\text{in}}$ to measurements is the best way to check for inconsistencies. The comparison shows that for most stations both $\hat{T}_a$ and $\hat{S}_{\text{in}}$ are in a reasonable agreement with the measurements. Stations at the northern edge of the Alps and on passes show realistic air temperatures and at the same time strong overestimation of global radiation. As previously discussed in this section, this picture reflects to a large degree biases in REMO or the inability of the RCM to consider small-scale processes.

[76] *Kotlarski et al.* [2009] have demonstrated that REMO is able to reproduce the temporal variability of annual means (T_a, P) well and consequently we refer to their study for a comparison of measured and modeled annual means.

7. Discussion

[77] The good correlations of modeled and measured mass balances shown in Figure 7 and auxiliary material Figure S2 confirm that REMO accurately reproduces the temporal variability of meteorological parameters [*Kotlarski et al.*, 2009]. The comparison of the 94-glaciers mean value to the *WGMS* [2007] and the *Huss et al.* [2008] data sets indicates that for a large sample size reasonable mean annual mass balances for the entire region are achieved using REMO and the present modeling approach. However, the shift of mean modeled mass balance for the four glaciers compared to the data of *Huss et al.* [2008] (Figure 7a) indicates systematic shifts of meteorological parameters at a local scale. Figures 7a and 8 indicate that the main source of such overestimations and underestimations lies in system-

atic errors in the accumulation calculation. This assumption is confirmed by *Kotlarski et al.* [2009], who state that REMO overestimates precipitation in the foreland and too little moisture reaches the main part of the Alps. Figure 6 shows that strongly negative mean balances mostly occur for glaciers in the interior parts of the Swiss Alps while the northernmost glaciers form a line of consistent positive or only slightly negative mass balances.

[78] The four glaciers sample size as well as the stake readings presented in Figure 8c mainly represent the interior part of the Alps and thus the comparison to the measurements indicates a general underestimation of accumulation. However, apart from local biases there are other potential reasons for this observation. (1) The comparison of annual means does not clearly show if precipitation is correct when it influences mass balance the most: according to *Kotlarski et al.* [2009], winter precipitation is somewhat underestimated by REMO. (2) Preferential deposition of snow on the smooth glacier surfaces as well as avalanche deposits resulting in enhanced accumulation on glaciers compared to the surroundings are not parameterized in the mass balance model. Including these processes, or evaluating the seasonality of the REMO output and modifying the downscaling scheme accordingly is beyond the scope of this study but should be addressed in future work.

[79] To sum up, the REMO data allow for a good representation of the annual variability of mass balance. Systematic overestimations and underestimations in modeled mass balances are mainly caused by local biases in precipitation, by simplifications made in the parameterization of accumulation and by the applied interpolators. In our case TPS preserves the characteristics of the REMO data satisfactory while IDW results in enhanced precipitation, global radiation and wet-day frequency. The good reproduction of melt is achieved because REMO correctly reproduces the strong correlation of T_a and elevation. Furthermore, REMO provides summer temperatures in good agreement to measurements [*Kotlarski et al.*, 2009] and seems to reproduce north-south and east-west gradients (see section 6.3) well. Global radiation is generally regarded as the most important source of melt energy for glaciers in the Alps. The chosen approach of clear-sky global radiation obtained from a radiation code and correction for cloudiness from REMO reproduces global radiation fairly well. Although Figure 9c shows strong overestimations by the model, the most apparent deviations do not impact on the model results: There are no glaciers located at the very northern edge of the Alps and local clouds on passes do mostly not affect the glaciers.

[80] Our study confirms the assumption from *Kotlarski et al.* [2009] that errors in the REMO data are too large yet to allow for an operational assessment of mass balance distribution without correction of the RCM biases. However, studies like the present one are able to provide feedback to climate modelers: Running a glacier mass balance model with RCM output is a test whether the RCM is able to reproduce the spatial distribution of the parameters governing glacier mass balance. Although such a test might have low confidence for individual glaciers, it is worthwhile to be conducted because very few meteorological measurements are available for the altitude of glacier occurrence and in the case of precipitation they are also related to large uncertainties.

8. Conclusions and Outlook

[81] In this study we presented a method to apply RCM data for high-resolution mass balance calculation over large glacier ensembles in complex alpine topography. In particular, we designed a method to convert meteorological output data, based on calculations of the RCM REMO, from a grid size of around 18 km to a cell size of 100 m, which is manageable with a regional-scale distributed mass balance model. For calculation and validation purposes, a careful selection of the glaciers using exclusion criteria such as debris cover, or calving is mandatory. Therefore, a selection of 94 glaciers, covering 50% of the total glacierized area, are used for mass balance calculation and 16 for validation. The main conclusion from this study is that the errors in the output of the RCM REMO are still too large to be used without any correction for the assessment of glacier mass balances in glacierized high-mountain environments. We believe, however, that the method could develop into a promising tool for future applications, especially in view of the fast improvements within the regional climate modeling community. The method could be applied to assess any possible impacts on the mass balances of large glacier samples due to a changing climate. In addition, the following specific conclusions are drawn:

[82] 1. The temporal variability of mass balance could be represented quite well. This is confirmed by the high correlations between variability of winter, summer and annual balances, resulting from a 24-year model run with measurements and the results of the study by *Huss et al.* [2008] and from the glacier monitoring network [*WGMS*, 2008].

[83] 2. Modeled and measured ablation rates are in good agreement mainly because air temperature is (1) strongly correlated with elevation and (2) spatially well produced by the RCM REMO. This has resulted in an overall good agreement with measurements at local climate stations.

[84] 3. In contrast to the well modeled ablation, measured accumulation is underestimated considerably. This is indicated by the systematic shifts of modeled mass balances in regions where measured annual and/or winter balances are available.

[85] 4. Overestimates and underestimates of the modeled mass balances are caused by a combined effect of (1) local RCM biases, (2) the parametrization of accumulation (e.g., no refreezing considered), (3) the application of different interpolations, and (4) the missing consideration of preferential snow deposition on smooth glacier surfaces.

[86] Possible future improvements of the here presented approach include the following.

[87] 1. The application of multimodel approaches, using the output of several different GCM/RCMs, would allow for (1) a better assessment of possible ranges of the mass balance calculations and (2) a better evaluation of the range of uncertainty associated with these models.

[88] 2. The mass balance model contains several simplifications that could be replaced by more detailed parameterizations, such as the inclusion of parameterized longwave radiation or turbulent fluxes.

[89] 3. The validation of the driving meteorological parameters should be refined by addressing seasonality of the different parameters. Subsequent bias correction for air temperature, global radiation (cloudiness) and precipitation could then deal with effects of seasonality.

[90] 4. An in-depth analysis of the deviations between modeled and measured accumulation is required. This should be done in combination with a correction of local biases in precipitation. Potential bias correction approaches are presented by, for example, *Wood et al.* [2004].

[91] 5. Consideration could be given to a variable glacier geometry.

[92] 6. Remote sensing could be used as a future validation tool for the model results (1) by the comparison of measured snow lines from satellites or aerial photography with the snow lines resulting from the transient model runs, (2) by introduction of surface albedo derived from satellites, and (3) by the comparison of modeled and measured decadal glacier volume changes.

[93] **Acknowledgments.** We gratefully acknowledge J. Oerlemans for providing the stake measurements from Morteratsch glacier, M. Huss for providing detailed mass balance data, and J. Corripio for making the global radiation code available to us. We want to thank W. Haeberli and N. Salzmann for their helpful comments on a draft of the paper as well as the Editor and three anonymous reviewers for their constructive comments that helped to significantly improve the clarity of the present study. MeteoSwiss provided the meteorological data. H. Machguth is supported by the Swiss Science Foundation (grant 20-117761). Figures 1, 3, 5, S1, and 6 are based upon the DHM25Level2 and the Vector200 data set from swisstopo (reproduced by permission, BA081414).

References

Arnold, N., I. Willis, M. Sharp, K. Richards, and W. Lawson (1996), A distributed surface energy balance model for a small valley glacier: I. development and testing for Haut Glacier d'Arolla, Valais, Switzerland, *J. Glaciol.*, *42*(140), 77–89.

Auer, I., et al. (2007), HISTALP—Historical instrumental climatological surface time series of the Greater Alpine Region, *Int. J. Climatol.*, *27*(1), 17–46.

Bhatt, U. S., J. Zhang, C. S. Lingle, and L. M. Phillips (2007), Examining glacier mass balances with a hierarchical modeling approach, *Comput. Sci. Eng.*, *9*(2), 60–67.

Böhm, R., I. Auer, M. Brunetti, M. Maugeri, T. Nanni, and W. Schöner (2001), Regional temperature variability in the European Alps: 1760–1998 from homogenized instrumental time series, *Int. J. Climatol.*, *21*(14), 1779–1801, doi:10.1002/joc.689.

Burrough, P. A., and R. A. McDonnell (2004), *Principles of Geographical Information Systems: Spatial Information Systems and Geostatistics*, Oxford Univ. Press, Oxford, U. K.

Cook, K., X. Yang, C. M. Carter, and B. N. Belcher (2003), A modelling system for studying climate controls mountain glaciers with application to the Patagonian icefields, *Clim. Change*, *56*, 339–367.

Corripio, J. (2003), Vectorial algebra algorithms for calculating terrain parameters from DEMs and solar radiation modelling in mountainous terrain, *Int. J. Geogr. Inf. Sci.*, *17*(1), 1–23, doi:10.1080/713811744.

Cryospheric Commission (1992–2008), Glaciological report: The Swiss glaciers, vols. 105–124, Swiss Acad. of Sci., Zurich, Switzerland.

Greuell, W., and C. Genthon (2004), Modelling land-ice surface mass balance, in *Mass Balance of the Cryosphere: Observations and Modelling of Contemporary and Future Changes*, edited by J. Bamber and A. Payne, pp. 117–168, Cambridge Univ. Press, New York.

Greuell, W., and J. Oerlemans (1986), Sensitivity studies with a mass balance model including temperature profile calculations inside the glacier, *Z. Gletscherkd. Glazialgeol.*, *22*, 101–124.

Greuell, W., W. Knap, and P. Smeets (1997), Elevational changes in meteorological variables along a mid-latitude glacier during summer, *J. Geophys. Res.*, *102*(D22), 25,941–25,954.

Huss, M., A. Bauder, M. Funk, and R. Hock (2008), Determination of the seasonal mass balance of four Alpine glaciers since 1865, *J. Geophys. Res.*, *113*, F01015, doi:10.1029/2007JF000803.

Iqbal, M. (1983), *An Introduction to Solar Radiation*, Academic Press, San Diego, Calif.

Jacob, D., et al. (2001), A comprehensive model intercomparison study investigating the water budget during the BALTEX-PIDCAP period, *Meteorol. Atmos. Phys.*, *77*(1–4), 19–43.

Kirchhofer, W., and B. Sevruk (2001), *Hydrological Atlas of Switzerland*, Landeshydrol. und Geol., Bern.

Klok, E. J., and J. Oerlemans (2002), Model study of the spatial distribution of the energy and mass balance of Morteratschgletscher, Switzerland, *J. Glaciol.*, *48*(163), 505–518.

Kotlarski, S., A. Block, U. Böhm, D. Jacob, K. Keuler, R. Knoche, D. Rechid, and A. Walter (2005), Regional climate model simulations as input for hydrological applications: Evaluation of uncertainties, *Adv. Geosci.*, *5*, 119–125.

Kotlarski, S., F. Paul, and D. Jacob (2009), Forcing a distributed glacier mass balance model with the regional climate model REMO, part I: RCM evaluation, *J. Clim.*, in press.

Machguth, H., O. Eisen, F. Paul, and M. Hoelzle (2006a), Strong spatial variability of snow accumulation observed with helicopter-borne GPR on two adjacent Alpine glaciers, *Geophys. Res. Lett.*, *33*, L13503, doi:10.1029/2006GL026576.

Machguth, H., F. Paul, M. Hoelzle, and W. Haeberli (2006b), Distributed glacier mass-balance modelling as an important component of modern multi-level glacier monitoring, *Ann. Glaciol.*, *43*, 335–343.

Machguth, H., R. S. Purves, J. Oerlemans, M. Hoelzle, and F. Paul (2008), Exploring uncertainty in glacier mass balance modelling with Monte Carlo simulation, *Cryosphere*, *2*, 191–204. (Available at http://www.the-cryosphere.net/2/191/2008/tc-2-191-2008.html)

Maisch, M., A. Wipf, B. Denneler, J. Battaglia, and C. Benz (2000), *Die Gletscher der Schweizer Alpen. Gletscherhochstand 1850, Aktuelle Vergletscherung, Gletscherschwund-Szenarien. Schlussbericht NFP 31-Projekt Nr. 4031-033412, (2. Auflage)*, 373 pp., vdf-Hochschulverlag ETH Zürich, Zurich, Switzerland.

Meerkötter, R., C. König, P. Bissolli, G. Gesell, and H. Mannstein (2004), A 14-year European cloud climatology from NOAA/AVHRR data in comparison to surface observations, *Geophys. Res. Lett.*, *31*, L15103, doi:10.1029/2004GL020098.

Müller, F., T. Callfisch, and G. Müller (1976), *Firn und Eis der Schweizer Alpen, Gletscherinventar.*, vol. 57, 174 pp., Geogr. Inst., ETH Zürich, Zurich, Switzerland.

Müller, H., and G. Kappenberger (1991), *Claridenfirn-Messungen 1914–1984, Zürcher Geogr. Schr.*, vol. 40, Geogr. Inst., ETH Zurich, Zurich, Switzerland.

Oerlemans, J. (2001), *Glaciers and Climate Change*, A. A. Balkema, Lisse, Netherland.

Paul, F. (2007), The new Swiss glacier inventory 2000—Application of remote sensing and GIS, Ph.D. thesis, Univ. of Zurich, Zurich, Switzerland.

Paul, F., A. Kääb, M. Maisch, T. W. Kellenberger, and W. Haeberli (2004), Rapid disintegration of Alpine glaciers observed with satellite data, *Geophys. Res. Lett.*, *31*, L21402, doi:10.1029/2004GL020816.

Paul, F., H. Machguth, and A. Kääb (2005), On the impact of glacier albedo under conditions of extreme glacier melt: The summer of 2003 in the Alps, *EARSeL eProc.*, *4*, 139–149.

Paul, F., H. Machguth, M. Hoelzle, N. Salzmann, and W. Haeberli (2008), Alpine-wide distributed glacier mass balance modelling: A tool for assessing future glacier change?, in *The Darkening Peaks: Glacial Retreat in Scientific and Social Context*, edited by B. Orlove, E. Wiegandt, and B. Luckman, pp. 111–125, Univ. of Calif. Press, Berkeley.

Plattner, C., L. N. Braun, and A. Brenning (2006), Spatial variability of snow accumulation on Vernagtferner, Austrian Alps, in winter 2003/2004, *Z. Gletscherkd. Glazialgeol.*, *39*, 43–57.

Radić, V., and R. Hock (2006), Modeling future glacier mass balance and volume changes using ERA-40 reanalysis and climate models: A sensitivity study at Storglaciaren, Sweden, *J. Geophys. Res.*, *111*, F03003, doi:10.1029/2005JF000440.

Ren, D., D. Karoly, and L. Leslie (2007), Temperate mountain glacier-melting rates for the period 2001–30: Estimates from three coupled GCM simulations for the greater Himalayas, *J. Appl. Meteorol. Climatol.*, *46*(6), 890–899.

Rohrer, M. (1989), Determination of the transition air temperature from snow to rain and intensity of precipitation, in *WMO/IAHS/ETH International Workshop on Precipitation Measurements St. Moritz, 1989 Switzerland*, edited by B. Sevruk, pp. 475–482, ETH Zürich, Zurich, Switzerland.

Rolland, C. (2003), Spatial and seasonal variations of air temperature lapse rates in alpine regions, *J. Clim.*, *16*, 1032–1046.

RSI Research Systems Inc. (2004), *IDL Reference Guide: July 2004 ed.*, RSI Research Systems Inc., Boulder, Colo.

Salzmann, N., C. Frei, P. Vidale, and M. Hoelzle (2007), The application of regional climate model output for the simulation of high-mountain permafrost scenarios, *Global Planet. Change*, *56*(1–2), 188–202, doi:10.1016/j.gloplacha.2006.07.006.

Schär, C., T. D. Davies, C. Frei, H. Wanner, M. Widmann, M. Wild, and H. C. Davies (1998), Current alpine climate, in *Views from the Alps: Regional Perspectives on Climate Change*, edited by P. Cebon et al., pp. 21–72, MIT Press, Cambridge, Mass.

Schneeberger, C., H. Blatter, A. Abe-Ouchi, and M. Wild (2003), Modelling changes in the mass balance of glaciers of the Northern Hemisphere for a transient $2 \times CO^2$ scenario, *J. Hydrol.*, *282*(1–4), 145–163.

Schwarb, M. (2000), The alpine precipitation climate: Evaluation of a high-resolution analysis scheme using comprehensive rain-gauge data, dissertation, Inst. for Clim. Res., ETH Zürich, Zurich, Switzerland.

Schwarb, M., C. Daly, C. Frei, and C. Schär (2001), *Hydrological Atlas of Switzerland*, Landeshydrol. und Geol., Bern.

Sevruk, B. (1985), Correction of precipitation measurements: Swiss experience, in *Proceedings Workshop on the Correction of Precipitation Measurements 1985 Zurich*, edited by B. Sevruk, pp. 187–193, ETH Zürich, Zurich, Switzerland.

Sevruk, B. (1997), Regional dependency of precipitation-altitude relationship in the Swiss Alps, *Clim. Change*, *36*, 355–369.

Stahl, K., R. D. Moore, J. M. Shea, D. Hutchinson, and A. J. Cannon (2008), Coupled modelling of glacier and streamflow response to future climate scenarios, *Water Resour. Res.*, *44*, W02422, doi:10.1029/2007WR005956.

Uppala, S., et al. (2005), The ERA-40 re-analysis, *Q. J. R. Meteorol. Soc.*, *131*(612), 2961–3012.

Van de Wal, R. S. M., and M. Wild (2001), Modelling the response of glaciers to climate change by applying volume-area scaling in combination with a high resolution GCM, *Clim. Dyn.*, *18*(3–4), 359–366.

Wipf, A. (1999), *Die Gletscher der Berner, Waadtländer und nördlichen Walliser Alpen. Eine regionale Studie über die Vergletscherung im Zeitraum "Vergangenheit" (Hochstand 1850), "Gegenwart" (Ausdehnung im Jahr 1973) und "Zukunft" (Gletscherschwund-Szenarien, 21. Jhdt.)*, *Phys. Geogr.*, vol. 40, 295 pp., Dep. of Geogr., Univ. of Zurich, Zurich, Switzerland.

Wood, A., L. Leung, V. Sridhar, and D. P. Lettenmaier (2004), Hydrologic implications of dynamical and statistical approaches to downscaling climate model outputs, *Clim. Change*, *62*, 189–216.

World Glacier Monitoring Service (WGMS) (2007), Glacier mass balance bulletin 2004–2005, *Bull. 9*, Univ. of Zurich, Zurich, Switzerland.

World Glacier Monitoring Service (WGMS) (2008), *Fluctuations of Glaciers 2000–2005*, vol. IX, edited by W. Haeberli et al., Univ. of Zurich, Zurich, Switzerland.

Zemp, M., R. Frauenfelder, W. Haeberli, and M. Hoelzle (2005), Worldwide glacier mass balance measurements: General trends and first results of the extraordinary year 2003 in central Europe, in *Materiali Gljaziologièeskix Issledovanij (Data of Glaciological Studies)*, vol. 99, pp. 3–12, Russ. Acad. of Sci., Moscow.

Zhang, J., U. Bhatt, W. V. Tangborn, and C. S. Lingle (2007), Climate downscaling for estimating glacier mass balances in northwestern North America: Validation with a USGS benchmark glacier, *Geophys. Res. Lett.*, *34*, L21505, doi:10.1029/2007GL031139.

M. Hoelzle, Department of Geoscience, University of Fribourg, CH-1700 Fribourg, Switzerland. (martin.hoelzle@unifr.ch)

S. Kotlarski, Institute for Atmospheric and Climate Science, ETH Zurich, CH-8092 Zurich, Switzerland. (sven.kotlarski@env.ethz.ch)

H. Machguth and F. Paul, Physical Geography Division, Department of Geography, University of Zurich, Winterthurerstraaße 190, CH-8057 Zurich, Switzerland. (horst.machguth@geo.uzh.ch; frank.paul@geo.uzh.ch)